Superfluidity and collective modes in a uniform gas of Fermi atoms with a Feshbach resonance

Y. Ohashi[1] and A. Griffin[2]
[1]*Institute of Physics, University of Tsukuba, Ibaraki 305, Japan*
[2]*Department of Physics, University of Toronto, Toronto, Ontario, Canada M5S 1A7*
(Received 10 February 2003; published 30 June 2003)

We investigate strong-coupling superfluidity in a uniform two-component gas of ultracold Fermi atoms attractively interacting via quasimolecular bosons associated with a Feshbach resonance. This interaction is tunable by the threshold energy 2ν of the Feshbach resonance, becoming large as 2ν is decreased (relative to $2\varepsilon_F$, where ε_F is the Fermi energy of one component). In recent work, we showed that the enhancement of this tunable pairing interaction naturally leads to the BCS-BEC (Bose-Einstein condensation) crossover, where the character of the superfluid phase transition changes from the BCS type to a BEC of composite bosons consisting of preformed Cooper-pairs and Feshbach-induced molecules. In this paper, we extend our previous work and study both the quasiparticles and the collective dynamics of the superfluid phase below the phase-transition temperature T_c, limiting ourselves to a uniform gas. We show how the superfluid order parameter changes from the Cooper-pair amplitude Δ to the square root of the number of condensed molecules (ϕ_m) associated with the Feshbach resonance, as the threshold energy 2ν is lowered. In the intermediate coupling regime, the superfluidity is shown to be characterized by an order parameter consisting of a superposition of Δ and ϕ_m. We also discuss the Goldstone mode associated with superfluidity, and show how its character smoothly changes from the Anderson-Bogoliubov phonon in the BCS regime to the Bogoliubov phonon in the BEC regime in the BCS-BEC crossover. The velocity of this Goldstone phonon mode is shown to strongly depend on the value of 2ν. We also show that this Goldstone mode appears as a resonance in the spectrum of the density-density correlation function, which is experimentally accessible.

DOI: 10.1103/PhysRevA.67.063612 PACS number(s): 03.75.Kk, 03.75.Ss, 74.20.Mn

I. INTRODUCTION

One of the most challenging topics in current physics is the realization of superfluidity in a trapped atomic gas composed of two Fermi hyperfine states. A considerable experimental effort has already been made to cooldown Fermi atom gases, such as ^{6}Li and ^{40}K [1–5]. The temperature can now be lowered to $T\sim 0.2T_F$, where the Fermi gas should be highly degenerate and the observation of superfluid behavior seems imminent [6].

As a promising mechanism of BCS superfluidity with a high transition temperature T_c, making use of an atomic Feshbach resonance has attracted much attention [7–15]. The Feshbach resonance describes quasimolecular bosons, which can mediate a pairing interaction between Fermi atoms. This pairing interaction is tunable by the threshold energy 2ν of the Feshbach resonance, and can become strong as 2ν is decreased relative to twice the Fermi energy of the atoms. Using this strong paring interaction, one can hope to achieve a high value of T_c. Experimentally, the threshold energy 2ν can be controlled by a weak applied magnetic field. Very recently, this tunable interaction was observed in a Fermi gas of ^{40}K [16,17].

In our recent work [12–14], we pointed out the importance of fluctuations in the Cooper-channel in considering a high-T_c superfluidity originating from the strong pairing interaction associated with a Feshbach resonance. We extended the strong-coupling theory developed by Nozières and Schmitt-Rink [18–21], to include the effects of a Feshbach resonance and the associated quasimolecular bosons. We showed that these particle-particle fluctuations strongly suppress T_c from the value expected within the simple mean-field BCS theory. In addition, the character of the phase transition was shown to continuously change from the BCS type to a BEC (Bose-Einstein condensation) of composite bosons (consisting of preformed Cooper-pairs and long-lived Feshbach molecules) as the threshold energy 2ν is lowered. Our strong-coupling theory thus gave an upper limit of $T_c = 0.518T_F$ for a Fermi gas in a harmonic trap potential [both T_c and T_F are proportional to the averaged trap frequency $\bar{\omega}_0 \equiv (\omega_{0x}\omega_{0y}\omega_{0z})^{1/3}$] and $T_c = 0.218T_F$ for a uniform gas [12–14]. These values are simply the BEC transition temperatures, expressed in terms of the Fermi temperature T_F of one of the Fermi components.

In this paper, we investigate the BCS-BEC crossover in the superfluid state, extending our previous work [12–14] to the superfluid region below T_c. Going past the previous BCS mean-field approximation [9,22–24], we include strong fluctuations around the BCS mean-field solution. We clarify how the order parameter described by the Cooper-pair amplitude $\Delta = U\Sigma_{\boldsymbol{p}}\langle c_{-\boldsymbol{p}\downarrow}c_{\boldsymbol{p}\uparrow}\rangle$ in the weak-coupling BCS theory changes to the BEC order parameter related to the number of condensed bosons $\phi_m = \langle b_{\boldsymbol{q}=0}\rangle$ in the BCS-BEC crossover. Here, $c_{\boldsymbol{p}\sigma}$ is the annihilation operator of a Fermi atom in one of two hyperfine states ($\sigma = \uparrow, \downarrow$) and $b_{\boldsymbol{q}}$ is the annihilation operator of the boson molecule associated with the Feshbach resonance.

In the field of trapped ultracold Fermi gases, a crucial issue is to determine a clear unambiguous signature for superfluidity [6,25–28]. Another important problem is how to experimentally track the system in the BCS-BEC crossover region. In this regard, the study of the Goldstone collective mode is very useful since it is deeply related to the sponta-

neous breakdown of the gauge symmetry associated with the superfluid phase transition. The Goldstone mode is known as the Anderson-Bogoliubov mode in the BCS state [29], while it is the Bogoliubov phonon in the BEC phase [30]. In this paper, we discuss how these collective modes change from one to the other as we go through the BCS-BEC crossover. We show that the velocity of the Goldstone phonon v_ϕ strongly depends on 2ν, and thus it offers a way of observing the BCS-BEC crossover phenomenon by tuning the threshold energy 2ν in a cigar-shaped trap (where the gas is fairly uniform in the axial direction). We also show that the Goldstone mode appears as a resonance in the spectrum of the density-density correlation function.

The present paper only considers the superfluid phase in a uniform two-component Fermi gas with an attractive interaction. In Ref. [14], we discussed the same model at and above the superfluid transition temperature for a trapped gas, using the local-density approximation (LDA). The extension of the present work to an inhomogeneous trapped gas will be considered in the future. As well known, the low-energy collective modes in a trapped atomic gas (Fermi or Bose) are strongly altered by the trap potential. However, the equivalent of the Goldstone phonon modes we discuss in this paper also arise in trapped two-component Fermi gases. These low-energy collective modes have been extensively discussed in the recent literature [31–33] for the weak-coupling BCS limit. In this paper, we discuss the physics of the Goldstone phonon mode as a function of the threshold energy 2ν. A similar analysis remains to be done for the collective modes of a trapped Fermi gas in the BCS-BEC crossover region.

This paper is organized as follows. In Sec. II, we present our coupled fermion-boson model. We explain how to include the strong-coupling (fluctuation) effect originating from the Feshbach resonance in Sec. III. In Sec. IV, we consider the Goldstone mode. We first derive correlation functions describing Cooper-pair fluctuations, as well as a renormalized boson Green's function for quasimolecules associated with the Feshbach resonance, using the Hartree-Fock random-phase approximation (HF-RPA). The Goldstone mode is then obtained from their poles. In Sec. V, we discuss the BCS-BEC crossover below T_c based on our numerical results. We also discuss the BCS-BEC crossover behavior of the order parameter and the Goldstone phonon mode, as a function of 2ν. In Sec. VI, we discuss the coupling of the Goldstone mode with density fluctuations. Section VII gives a summary and a brief discussion of trapped Fermi gases.

II. COUPLED FERMION-BOSON MODEL

We consider a gas of Fermi atoms composed of two atomic hyperfine states, coupled to molecular two-particle state. We describe the two hyperfine states using a pseudospin variable σ $(=\uparrow, \downarrow)$. The coupled fermion-boson model Hamiltonian is given by [7–15,22–24]

$$\begin{aligned}\mathcal{H}=&\sum_{\boldsymbol{p}\sigma}\ \varepsilon_{\boldsymbol{p}}c^{\dagger}_{\boldsymbol{p}\sigma}c_{\boldsymbol{p}\sigma}\\&-U\sum_{\boldsymbol{p},\boldsymbol{p}',\boldsymbol{q}}\ c^{\dagger}_{\boldsymbol{p}+\boldsymbol{q}/2\uparrow}c^{\dagger}_{-\boldsymbol{p}+\boldsymbol{q}/2\downarrow}c_{-\boldsymbol{p}'+\boldsymbol{q}/2\downarrow}c_{\boldsymbol{p}'+\boldsymbol{q}/2\uparrow}\\&+\sum_{\boldsymbol{q}}\ [\varepsilon_{B\boldsymbol{q}}+2\nu]b^{\dagger}_{\boldsymbol{q}}b_{\boldsymbol{q}}\\&+g_{\mathrm{r}}\sum_{\boldsymbol{p},\boldsymbol{q}}\ [b^{\dagger}_{\boldsymbol{q}}c_{-\boldsymbol{p}+\boldsymbol{q}/2\downarrow}c_{\boldsymbol{p}+\boldsymbol{q}/2\uparrow}+\mathrm{H.c.}].\end{aligned}\tag{2.1}$$

Here, a Fermi atom and a quasimolecular boson associated with the Feshbach resonance are, respectively, described by the destruction operators $c_{\boldsymbol{p}\sigma}$ and $b_{\boldsymbol{q}}$. The kinetic energy of a Fermi atom is $\varepsilon_{\boldsymbol{p}}\equiv p^2/2m$ and $\varepsilon_{B\boldsymbol{q}}+2\nu\equiv q^2/2M+2\nu$ is the excitation spectrum of the b-molecular bosons. Here, 2ν represents the lowest excitation energy of b bosons, also referred to as the threshold energy of the Feshbach resonance. The last term in Eq. (2.1) describes the Feshbach resonance with a coupling constant g_{r}, which describes how a b molecule can dissociate into two Fermi atoms and how two Fermi atoms can form one b boson. The Hamiltonian in Eq. (2.1) also includes an attractive fermion-fermion interaction $-U$ (<0) arising from nonresonant processes [9].

Since one b Bose molecule consists of two Fermi atoms, the boson mass $M=2m$ and the conservation of the total number of particles N imposes the relation

$$N=\sum_{\boldsymbol{p}\sigma}\ \langle c^{\dagger}_{\boldsymbol{p}\sigma}c_{\boldsymbol{p}\sigma}\rangle+2\sum_{\boldsymbol{q}}\ \langle b^{\dagger}_{\boldsymbol{q}}b_{\boldsymbol{q}}\rangle.\tag{2.2}$$

We incorporate this crucial constraint into the model Hamiltonian in Eq. (2.1) using a chemical potential, $\mathcal{H}\equiv H-\mu N$. The resulting grand-canonical Hamiltonian $\mathcal{H}$ has the same form as Eq. (2.1), except that the kinetic energies of Fermi atoms and b bosons are replaced by $\varepsilon_{\boldsymbol{p}}\rightarrow\xi_{\boldsymbol{p}}\equiv\varepsilon_{\boldsymbol{p}}-\mu$ and $\varepsilon_{B\boldsymbol{q}}+2\nu\rightarrow\xi_{B\boldsymbol{q}}\equiv\varepsilon_{B\boldsymbol{q}}+2\nu-2\mu$, respectively. In the latter replacement, the factor of 2 in 2μ reflects the fact that one b boson consists of two Fermi atoms.

In this paper, we investigate strong-coupling effects in the superfluid phase, as well as the Goldstone mode associated with superfluidity in the BCS-BEC crossover region. As a start, we consider a uniform Fermi gas and leave the effect of a trapping potential to future work. In this regard, we have shown in Refs. [12–14] that while a trap potential enhances the transition temperature T_c in the BEC regime, the qualitative behavior of T_c in the BCS-BEC crossover is not very different from a uniform Fermi gas. Within weak-coupling BCS theory, several papers have discussed collective excitations in a trapped Fermi gas with attractive interactions. (See, for example, Refs. [31–33].)

When the Feshbach coupling term is absent in Eq. (2.1), the fermions and b bosons are decoupled from each other. In this limit, a BCS superfluid phase transition of Fermi atoms and BEC transition of b bosons can occur, at different temperatures. These two superfluid phases are, respectively, described by independent order parameters

$$\Delta \equiv U \sum_{\boldsymbol{p}} \langle c_{-\boldsymbol{p}\downarrow} c_{\boldsymbol{p}\uparrow} \rangle,$$

$$\phi_{\mathrm{m}} \equiv \langle b_{\boldsymbol{q}=0} \rangle. \tag{2.3}$$

On the other hand, when the Feshbach resonance term is present ($g_{\mathrm{r}} \neq 0$), we find the following identity in the equilibrium state:

$$0 = i \frac{d\phi_{\mathrm{m}}}{dt} = i \left\langle \frac{db_0}{dt} \right\rangle = \langle [b_0, \mathcal{H}] \rangle = (2\nu - 2\mu)\phi_{\mathrm{m}} + \frac{g_{\mathrm{r}}}{U}\Delta. \tag{2.4}$$

Equation (2.4) gives [8,9]

$$\phi_{\mathrm{m}} = -\frac{g_{\mathrm{r}}}{2\nu - 2\mu} \frac{\Delta}{U}. \tag{2.5}$$

This last result shows that the BEC order parameter ϕ_{m} and the Cooper-pair order parameter Δ are no longer independent, due to the hybridization induced by the Feshbach resonance g_{r}. Both Δ and ϕ_{m} are finite in the superfluid phase, and there is a unique superfluid phase transition in this coupled fermion-boson model.

For later convenience, we define the following composite order parameter [8,9,12]:

$$\tilde{\Delta} \equiv \Delta - g_{\mathrm{r}} \phi_{\mathrm{m}}. \tag{2.6}$$

We will find that $\tilde{\Delta}$ corresponds to the excitation energy gap in the spectrum of fermion quasi-particles below T_{c} in the BCS-BEC crossover regime.

III. STRONG-COUPLING EFFECTS ON SUPERFLUIDITY

A. Review of strong-coupling theory for T_{c}

In this section, we review the strong-coupling theory for T_{c} discussed in our previous papers [12–14]. This formulation is extended to the region below T_{c} in the following sections.

In previous work [12–14], we extended the strong-coupling theory developed by Nozières and Schmitt-Rink [18] to the coupled fermion-boson model in Eq. (2.1). The equation for T_{c} was obtained by using the Thouless criterion, which states that the superfluid phase transition occurs when the particle-particle vertex function $\Gamma(\mathbf{q}, \omega)$ describing the Cooper-channel develops a pole at $\mathbf{q} = \omega = 0$. Within the t-matrix approximation in terms of $-U$ and g_{r} described diagrammatically in Fig. 1(a), this equation for T_{c} is given by

$$1 = U_{\mathrm{eff}} \sum_{\boldsymbol{p}} \frac{\tanh 2\xi_{\boldsymbol{p}}/2T_{\mathrm{c}}}{2\xi_{\boldsymbol{p}}}, \tag{3.1}$$

where

$$U_{\mathrm{eff}} \equiv U + g_{\mathrm{r}}^2 \frac{1}{2\nu - 2\mu} \tag{3.2}$$

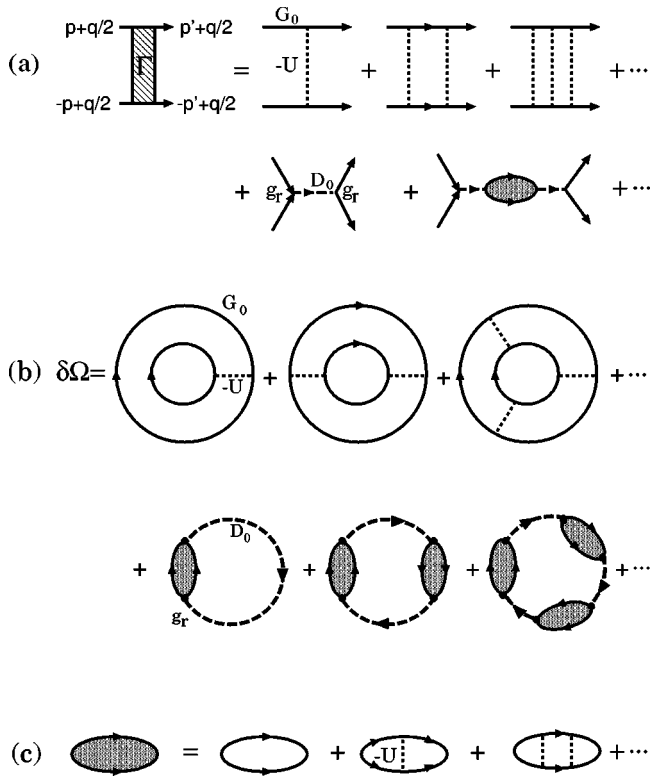

FIG. 1. (a) t-matrix approximation for the particle-particle scattering vertex Γ at T_{c}. The solid line represents the fermion Green's function. The first line in the figure involves the ladder processes by nonresonant interaction $-U$, while the second line involves the Feshbach resonance described by the b-boson Green's function D_0. (b) Fluctuation contribution to the thermodynamic potential Ω at T_{c}. The first line represents the Cooper-channel particle-particle fluctuations associated with the nonresonant interaction $-U$, and the second line describes the effect of the Feshbach resonance coupling g_{r}. (c) The shaded bubble includes ladder diagram scattering processes by $-U$.

is an effective pairing interaction. The last term in Eq. (3.2) describes the interaction mediated by b bosons associated with the Feshbach resonance. Equation (3.1) is formally identical to the equation for T_{c} in an ordinary weak-coupling BCS theory. However, the chemical potential μ in the kinetic energy $\xi_{\boldsymbol{p}} = \varepsilon_{\boldsymbol{p}} - \mu$ of the Fermi atoms can deviate strongly from ε_{F} as one approaches the BEC regime (where ε_{F} is the bare Fermi energy of one spin component). This contrasts with simple BCS theory, where one finds that $\mu \simeq \varepsilon_{\mathrm{F}}$.

The chemical potential μ is determined by the equation for the total number of Fermi atoms, using the identity $N = -\partial\Omega/\partial\mu$. We include the effect of fluctuations in the Cooper-channel [the first line in Fig. 1(b)] as well as the Feshbach resonance [the second line in Fig. 1(b)] in the thermodynamic potential Ω. The resulting equation relating μ and N is

$$N = N_{\mathrm{F}}^0 + 2N_{\mathrm{B}}^0 - \frac{1}{\beta} \sum_{\mathbf{q}, \nu_n} e^{i\delta\nu_n} \frac{\partial}{\partial\mu} \times \ln[1 - [U - g_{\mathrm{r}}^2 D_0(\mathbf{q}, i\nu_n)]\Pi(\mathbf{q}, i\nu_n)]. \tag{3.3}$$

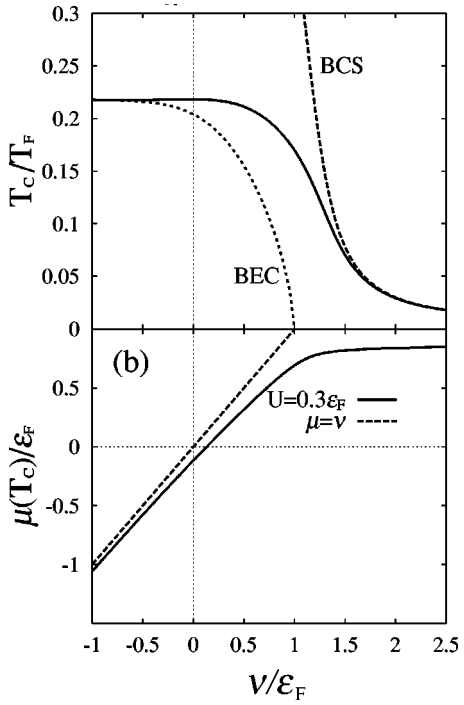

FIG. 2. (a) The BCS-BEC crossover at the superfluid phase-transition temperature T_c in a gas of Fermi atoms with a Feshbach resonance, as a function of the threshold parameter ν. We take $g_r/\varepsilon_F=0.6$, $U/\varepsilon_F=0.6$ and $\omega_c/\varepsilon_F=2$. BCS labels the result in the absence of fluctuation effects and BEC gives T_c of a Bose-condensed gas of $N/2$ molecules of mass $M=2m$. (b) The chemical potential μ at T_c, shown as a function of ν. These results are from Ref. [12].

Here, $\beta=1/T$ is the inverse of temperature, $N_F^0\equiv 2\Sigma_{\boldsymbol{p}} f(\xi_{\boldsymbol{p}})$ and $N_B^0\equiv\Sigma_{\boldsymbol{q}} n_B(\xi_{B\boldsymbol{q}})$, where $f(\varepsilon)$ and $n_B(\varepsilon)$ represent the Fermi and Bose distribution functions, respectively. The last term in Eq. (3.3) describes the fluctuation contribution to N. The b-boson Green's function is given by

$$D_0(\mathbf{r},i\nu_n)\equiv\frac{1}{i\nu_n-\xi_{B\boldsymbol{q}}}, \tag{3.4}$$

where the Bose Matsubara frequency is $\nu_n=2n\pi T(n=0,\pm1,\pm2,\ldots)$. $\Pi(\mathbf{q},i\nu_n)$ is the correlation function of the Cooper-pair field operator $\hat{F}_{\boldsymbol{q}}\equiv\Sigma_{\boldsymbol{p}} c_{-\boldsymbol{p}+\boldsymbol{q}/2\downarrow}c_{\boldsymbol{p}+\boldsymbol{q}/2\uparrow}$, given by

$$\begin{aligned}\Pi(\mathbf{q},i\nu_n)&\equiv\int_0^\beta d\tau e^{i\nu_n\tau}\langle T_\tau\{\hat{F}_{\boldsymbol{q}}(\tau)\hat{F}_{\boldsymbol{q}}^\dagger(0)\}\rangle\\&=\frac{1}{\beta}\sum_{\boldsymbol{p},\omega_m}G_0\left(\mathbf{p}+\frac{\mathbf{q}}{2},i\omega_m+i\nu_n\right)G_0\left(-\mathbf{p}+\frac{\mathbf{q}}{2},i\omega_m\right)\\&=\sum_{\boldsymbol{p}}\frac{1-f(\xi_{\boldsymbol{p}+\boldsymbol{q}/2})-f(\xi_{\boldsymbol{p}-\boldsymbol{q}/2})}{\xi_{\boldsymbol{p}+\boldsymbol{q}/2}+\xi_{\boldsymbol{p}-\boldsymbol{q}/2}-i\nu_n}.\end{aligned} \tag{3.5}$$

Physically, $\Pi(\mathbf{q},i\nu_n)$ describes fluctuations of Cooper pairs in the normal phase. $G_0(\mathbf{q},i\omega_m)$ is a fermion thermal Green's function defined by

$$G_0(\mathbf{q},i\omega_m)=\frac{1}{i\omega_m-\xi_{\boldsymbol{p}}}, \tag{3.6}$$

where the Fermi Matsubara frequency is $\omega_m=(2m+1)\pi T$ $(m=0,\pm1,\pm2,\ldots)$.

The coupled equations (3.1) and (3.3) determine T_c and μ self-consistently. In calculating these equations, a cutoff is necessary to make the momentum summation converge. In Refs. [12–14], we simply introduced a Gaussian cutoff $e^{-\varepsilon_p^2/\omega_c^2}$, which is also used in this paper.

The self-consistent solution (T_c and μ) of these coupled equations is summarized in Fig. 2. When $\nu\gg\varepsilon_F$, since the chemical potential is at most $\mu\lesssim\varepsilon_F$, the Feshbach-induced contribution to the pairing interaction $g_r^2/(2\nu-2\mu)$ in Eq. (3.2) is small. In this regime, Fig. 2(a) shows that the superfluid phase transition is well described by the weak-coupling BCS theory with a (weak) pairing interaction $-U$. In addition, we see that $\mu\simeq\varepsilon_F$, as shown in Fig. 2(b). However, the chemical potential μ gradually deviates from ε_F as the threshold energy 2ν is lowered towards $2\varepsilon_F$ and below. In particular, one finds μ approaches ν when $\nu<0$. In this regime, the Feshbach-induced pairing interaction $g_r^2/(2\nu-2\mu)$ in Eq. (3.2) is large, and T_c deviates significantly from the prediction of weak-coupling BCS theory, as shown in Fig. 2(a). Since 2ν is the lowest excitation energy of b bosons and their chemical potential is 2μ, the situation $2\nu=2\mu$, realized in the limit of large negative values of ν/ε_F, is equivalent to the condition of BEC in a noninteracting Bose gas. Indeed, Fig. 2(a) shows that T_c corresponds precisely to the transition temperature of a free Bose gas of $N/2$ atoms when $\nu/\varepsilon_F<-1$. These results show that the BCS-BEC crossover starts in the region where $2\nu=2\varepsilon_F$, at least for small values of g_r. This crossover phenomenon can be simply controlled by the threshold energy 2ν of the Feshbach resonance.

We note that when one uses a large value of the Feshbach coupling parameter g_r, there is a small peak in T_c in the crossover to the BEC phase [15]. However, as we have discussed in Sec. VII of Ref. [14], this peak is spurious, being a result of not including the fermion self-energy due to coupling to the Cooper-pair bound states. This was first pointed out in the context of a uniform electron gas by Haussmann [34].

B. Strong-coupling theory below T_c

In order to formulate the analogous strong-coupling theory below T_c, we separate out the fluctuations of Cooper-pairs and condensed b bosons around their mean-field values denoted by Δ and ϕ_m, respectively [35,36]. For this purpose, we write $\hat{F}_{\boldsymbol{q}}=\langle\hat{F}_{\boldsymbol{q}=0}\rangle\delta_{\boldsymbol{q},0}+\delta\hat{F}_{\boldsymbol{q}}$ and $\hat{b}_{\boldsymbol{q}}=\phi_m\delta_{\boldsymbol{q},0}+\delta b_{\boldsymbol{q}}$, where $\hat{F}_{\boldsymbol{q}}$ is defined before Eq. (3.5). Separating out the fluctuation contribution to the Hamiltonian in Eq. (2.1), we obtain

$$\mathcal{H}=\frac{\tilde{\Delta}^2}{U_{\rm eff}}+\sum_{\boldsymbol{p}}\ \xi_{\boldsymbol{p}}+\sum_{\boldsymbol{p}}\ \hat{\Psi}^{\dagger}_{\boldsymbol{p}}[\xi_{\boldsymbol{p}}\tau_3-\tilde{\Delta}\tau_1]\hat{\Psi}_{\boldsymbol{p}}+\sum_{\boldsymbol{q}}\ \xi_{B\boldsymbol{q}}b^{\dagger}_{\boldsymbol{q}}b_{\boldsymbol{q}}$$
$$+\frac{g_{\rm r}}{2}\sum_{\boldsymbol{q}}\ [b^{\dagger}_{\boldsymbol{q}}\rho^{-}_{\boldsymbol{q}}+b_{\boldsymbol{q}}\rho^{+}_{\boldsymbol{q}}]-\frac{U}{4}\sum_{\boldsymbol{q}}\ [\rho_{1\boldsymbol{q}}\rho_{1-\boldsymbol{q}}+\rho_{2\boldsymbol{q}}\rho_{2-\boldsymbol{q}}]. \tag{3.7}$$

Here, we have introduced the Nambu field operator for Fermi atoms as $\hat{\Psi}^{\dagger}_{\boldsymbol{p}}\equiv(c^{\dagger}_{\boldsymbol{p}\uparrow},c_{-\boldsymbol{p}\downarrow})$ and the corresponding 2×2 Pauli matrices τ_i $(i=1,2,3)$ acting on the particle-hole space [37]. The order parameter $\tilde{\Delta}$ is defined by Eqs. (2.3) and (2.6), which we can take to be real and proportional to $\tau_1=\left(\begin{smallmatrix}0&1\\1&0\end{smallmatrix}\right)$ without loss of generality. In Eq. (3.7) and the subsequent discussion, we use the generalized density operators $\rho^{\pm}_{\boldsymbol{q}}\equiv\rho_{1\pm\boldsymbol{q}}\pm i\rho_{2\pm\boldsymbol{q}}$, where

$$\rho_{j\boldsymbol{q}}\equiv\sum_{\boldsymbol{p}}\ \Psi^{\dagger}_{\boldsymbol{p}+\boldsymbol{q}/2}\tau_j\Psi_{\boldsymbol{p}-\boldsymbol{q}/2}\,. \tag{3.8}$$

We note that $\rho_{3\boldsymbol{q}}=\Sigma_{\boldsymbol{p},\sigma}c^{\dagger}_{\boldsymbol{p}+\boldsymbol{q}/2,\sigma}c_{\boldsymbol{p}-\boldsymbol{q}/2,\sigma}$ is the ordinary density-fluctuation operator. Similarly, one has

$$\rho_{1\boldsymbol{q}}=\sum_{\boldsymbol{p}}\ [c_{-\boldsymbol{p}-\boldsymbol{q}/2\downarrow}c_{\boldsymbol{p}-\boldsymbol{q}/2\uparrow}+c^{\dagger}_{\boldsymbol{p}+\boldsymbol{q}/2\uparrow}c^{\dagger}_{-\boldsymbol{p}+\boldsymbol{q}/2\downarrow}],$$

$$\rho_{2\boldsymbol{q}}=i\sum_{\boldsymbol{p}}\ [c_{-\boldsymbol{p}-\boldsymbol{q}/2\downarrow}c_{\boldsymbol{p}-\boldsymbol{q}/2\uparrow}-c^{\dagger}_{\boldsymbol{p}+\boldsymbol{q}/2\uparrow}c^{\dagger}_{-\boldsymbol{p}+\boldsymbol{q}/2\downarrow}], \tag{3.9}$$

and hence

$$\rho^{+}_{\boldsymbol{q}}=2\sum_{\boldsymbol{p}}\ c^{\dagger}_{\boldsymbol{p}+\boldsymbol{q}/2\uparrow}c^{\dagger}_{-\boldsymbol{p}+\boldsymbol{q}/2\downarrow},\quad \rho^{-}_{\boldsymbol{q}}=2\sum_{\boldsymbol{p}}\ c_{-\boldsymbol{p}-\boldsymbol{q}/2\downarrow}c_{\boldsymbol{p}-\boldsymbol{q}/2\uparrow}\,. \tag{3.10}$$

The operators $\rho_{1\boldsymbol{q}}$ and $\rho_{2\boldsymbol{q}}$ describe, respectively, the amplitude and phase fluctuations of Cooper-pair field fluctuation operator $\hat{F}_{\boldsymbol{q}}$. In Eq. (3.7), the fermion-fermion interaction is seen to be neatly expressed as the sum of interactions between the amplitude fluctuations $[-(U/4)\Sigma_{\boldsymbol{q}}\rho_{1\boldsymbol{q}}\rho_{1-\boldsymbol{q}}]$ and phase fluctuations $[-(U/4)\Sigma_{\boldsymbol{q}}\rho_{2\boldsymbol{q}}\rho_{2-\boldsymbol{q}}]$. The Feshbach resonance is also expressed as an interaction between the b-bosons and the fluctuations described by $\rho^{\pm}_{\boldsymbol{q}}$. In Eq. (3.7), we have simply written $\rho_{1\boldsymbol{q}=0}-\langle\rho_{1\boldsymbol{q}=0}\rangle\to\rho_{1\boldsymbol{q}=0}$ and $b_{\boldsymbol{q}=0}-\phi_{\rm m}\to b_{\boldsymbol{q}=0}$.

Within the mean-field approximation described by the third term in Eq. (3.7), the fermion thermal Green's function is conveniently discussed in terms of a 2×2 matrix Green's function

$$\hat{G}(\mathbf{p},i\omega_m)=\frac{1}{i\omega_m-\xi_{\boldsymbol{p}}\tau_3+\tilde{\Delta}\tau_1}=-\frac{i\omega_m+\xi_{\boldsymbol{p}}\tau_3-\tilde{\Delta}\tau_1}{\omega_m^2+E_{\boldsymbol{p}}^2}. \tag{3.11}$$

Here, $E_{\boldsymbol{p}}\equiv\sqrt{\xi_{\boldsymbol{p}}^2+\tilde{\Delta}^2}$ is the energy spectrum of fermion quasiparticles below $T_{\rm c}$, which we shall call the BCS-Bogoliubov quasiparticle spectrum. Equation (3.11) reduces to the mean-field BCS matrix Green's function [37] when the composite order parameter $\tilde{\Delta}$ is replaced by Δ. The off-diagonal (static) self-energy $\hat{\Sigma}_{\rm F}\equiv-\tilde{\Delta}\tau_1$ comes from the mean-field term $\tilde{\Delta}\tau_1$ appearing in the Hamiltonian in Eq. (3.7). This self-energy corresponds to the mean-field diagrams shown in Fig. 3,

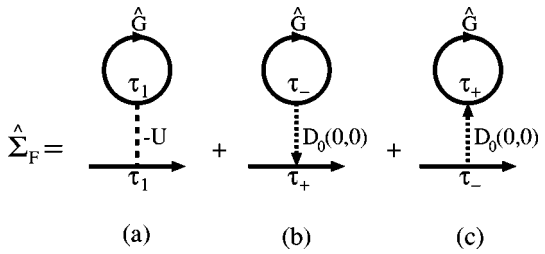

FIG. 3. The off-diagonal static mean-field self-energies in the 2×2-matrix fermion Green's function $\hat{G}(\mathbf{p},i\omega_m)$ given in Eq. (3.11). Diagram (a) gives the contribution from the nonresonant interaction $-U$. Diagrams (b) and (c) include the pairing interaction mediated by a Feshbach molecular boson described by the b-boson Green's function $D_0(\mathbf{q},i\nu_n)$. In the diagrams (b) and (c), $\tau_{\pm}\equiv\tau_1\pm i\tau_2$. Since $\hat{G}(\mathbf{p},i\omega)$ in Eq. (3.11) does not have a τ_2 component, a diagram similar to (a), where τ_1 is replaced by τ_2, is absent.

$$\hat{\Sigma}_{(\rm a)}=-\tau_1\frac{U}{2\beta}\sum_{\mathbf{p},\omega_m}{\rm Tr}[\tau_1\hat{G}(\mathbf{p},i\omega_m)]$$
$$=-\tau_1U\sum_{\boldsymbol{p}}\ \frac{\tilde{\Delta}}{2E_{\boldsymbol{p}}}\tanh\frac{\beta}{2}E_{\boldsymbol{p}},$$

$$\hat{\Sigma}_{(\rm b)}=-\tau_+\frac{g_{\rm r}^2}{4\beta}D_0(0,0)\sum_{\mathbf{p},\omega_m}{\rm Tr}[\tau_-\hat{G}(\mathbf{p},i\omega_m)]$$
$$=-\tau_+\frac{g_{\rm r}^2}{2\nu-2\mu}\sum_{\boldsymbol{p}}\ \frac{\tilde{\Delta}}{4E_{\boldsymbol{p}}}\tanh\frac{\beta}{2}E_{\boldsymbol{p}},$$

$$\hat{\Sigma}_{(\rm c)}=-\tau_-\frac{g_{\rm r}^2}{4\beta}D_0(0,0)\sum_{\mathbf{p},\omega_m}{\rm Tr}[\tau_+\hat{G}(\mathbf{p},i\omega_m)]$$
$$=-\tau_-\frac{g_{\rm r}^2}{2\nu-2\mu}\sum_{\boldsymbol{p}}\ \frac{\tilde{\Delta}}{4E_{\boldsymbol{p}}}\tanh\frac{\beta}{2}E_{\boldsymbol{p}}, \tag{3.12}$$

where $\tau_{\pm}\equiv\tau_1\pm i\tau_2$. In Eq. (3.12), $\hat{\Sigma}_{(\rm b)}$ and $\hat{\Sigma}_{(\rm c)}$ include the pairing interaction mediated by a Feshbach b molecule described by the propagator D_0. $\hat{\Sigma}_{(\rm a)}$ comes from the (weak) nonresonant interaction $-U$. The matrix self-energy $\hat{\Sigma}_{\rm F}=\hat{\Sigma}_{(\rm a)}+\hat{\Sigma}_{(\rm b)}+\hat{\Sigma}_{(\rm c)}$ sums up to give

$$\hat{\Sigma}_{\rm F}=-\tau_1U_{\rm eff}\sum_{\boldsymbol{p}}\ \frac{\tilde{\Delta}}{2E_{\boldsymbol{p}}}\tanh\frac{\beta}{2}E_{\boldsymbol{p}}=-\tau_1\tilde{\Delta}. \tag{3.13}$$

In the last expression, we have used the gap equation in Eq. (3.16).

Using Eq. (3.11), we see that

$$\Delta \equiv U\sum_{\boldsymbol{p}} \langle c_{-\boldsymbol{p}\downarrow} c_{\boldsymbol{p}\uparrow}\rangle = \frac{U}{2\beta}\sum_{\boldsymbol{p},\omega_m} \mathrm{Tr}[\tau_1 \hat{G}(\mathbf{p}, i\omega_m)]$$

$$= U\sum_{\boldsymbol{p}} \frac{\tilde{\Delta}}{2E_{\boldsymbol{p}}}\tanh\frac{\beta}{2}E_{\boldsymbol{p}}. \tag{3.14}$$

The order parameters ϕ_{m} and Δ can be obtained in terms of $\tilde{\Delta}$ by using Eqs. (2.5) and (2.6), to give

$$\Delta = \frac{U}{U_{\mathrm{eff}}}\tilde{\Delta},$$

$$\phi_{\mathrm{m}} = -\frac{g_{\mathrm{r}}}{2\nu - 2\mu}\frac{1}{U_{\mathrm{eff}}}\tilde{\Delta}. \tag{3.15}$$

The equation for the composite order parameter $\tilde{\Delta} = \Delta - g_{\mathrm{r}}\phi_{\mathrm{m}}$ can then be rewritten in the form

$$\tilde{\Delta} = U_{\mathrm{eff}}\sum_{\boldsymbol{p}} \frac{\tilde{\Delta}}{2E_{\boldsymbol{p}}}\tanh\frac{\beta}{2}E_{\boldsymbol{p}}, \tag{3.16}$$

where U_{eff} is defined in Eq. (3.2). This self-consistent equation has the same form as the BCS gap equation if we replace $\tilde{\Delta} \to \Delta$ and $\mu \to \varepsilon_{\mathrm{F}}$. We also note that Eq. (3.16) reduces to the T_{c} equation in Eq. (3.1) when $\tilde{\Delta} \to 0$ [12].

It is important to emphasize that the 2×2-matrix single-particle Green's function in Eq. (3.11) only includes self-energy effects arising from the (off-diagonal) static mean fields produced by the Cooper-pairs and the Bose-condensed *b* molecules. In the approximation we use in this paper, the frequency-dependent fermion self-energies associated with the order parameter collective modes are not included in Eq. (3.11). However, Eq. (3.11) does implicitly involve the self-consistent renormalized values of $\tilde{\Delta}$ and μ, as determined by the order parameter fluctuations (for further discussion of this kind of approximation, see Ref. [38]). An improved theory of the BCS-BEC crossover would be based on including the fermion self-energies arising from coupling to collective modes [34].

The chemical potential μ is determined from the equation for the total number of particles *N*. As in our discussion of the strong-coupling theory for T_{c} [12–14], we work with the thermodynamic potential Ω consisting of a static mean-field part ($\equiv \Omega_{\mathrm{MF}}$) and a fluctuation part ($\equiv \delta\Omega$) originating from the particle-particle Cooper channel, as modified by the Feshbach resonance. The self-consistent equation for *N* is given using the identity $N = -\partial\Omega/\partial\mu$. The mean-field part is easily obtained from the first four terms on the right-hand side in Eq. (3.7) [39],

$$\Omega_{\mathrm{MF}} = \frac{\tilde{\Delta}^2}{U_{\mathrm{eff}}} + \sum_{\boldsymbol{p}} (\xi_{\boldsymbol{p}} - E_{\boldsymbol{p}}) - 2T\sum_{\boldsymbol{p}} \ln[1 + e^{-\beta E_{\boldsymbol{p}}}]$$

$$+ T\sum_{\boldsymbol{q}} \ln[1 - e^{-\beta\xi_{B\boldsymbol{q}}}]. \tag{3.17}$$

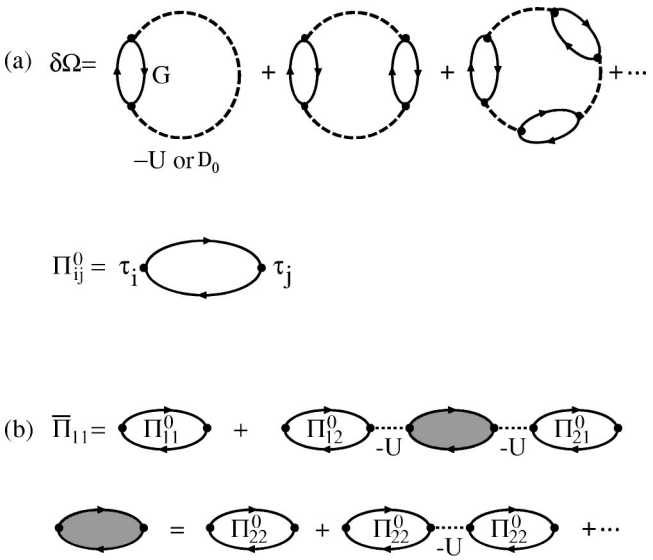

FIG. 4. (a) Fluctuation contribution $\delta\Omega$ to the thermodynamic potential below T_{c}. The bubble shows the correlation function Π^0_{ij}. (b) Correlation function of amplitude fluctuations $\overline{\Pi}_{11}$ involving a coupling with phase fluctuations described by the response function Π^0_{22}. The shaded bubble includes multiscattering processes by $-U$. Since the 2×2-matrix fermion Green's functions *G* are given in the Nambu representation, Π^0_{ij} is formally described as a particle-hole bubble diagram. (In contrast, Π is described by a particle-particle bubble diagram in Fig. 1 because the Nambu two-component representation is not used there.)

Our approximation for the fluctuation contribution $\delta\Omega$ below T_{c}, corresponding to the contribution at T_{c} shown in Fig. 1(b), is given diagrammatically in Fig. 4(a). Among the interaction terms in Eq. (3.7), we first carry out perturbative expansion in terms of $-(U/4)\Sigma_{\boldsymbol{q}}\rho_{2\boldsymbol{q}}\rho_{2-\boldsymbol{q}}$, which describes the interaction between the phase fluctuations of Δ. Summing up the loop-type diagrams in Fig. 4(a), we obtain the phase fluctuation contribution to $\delta\Omega$

$$\delta\Omega_2 = \frac{1}{2\beta}\sum_{\boldsymbol{q},\nu_n} \ln\left[1 + \frac{U}{2}\Pi^0_{22}(\mathbf{q}, i\nu_n)\right]. \tag{3.18}$$

In this ν_n summation and in the following equations, we omit the important convergence factor $e^{i\nu_n\delta}$, for simplicity of notation. The generalized density correlation function $\Pi^0_{22}(\mathbf{q}, i\nu_n)$ is defined by [35,36] $(i,j = 1,2,3)$

$$\Pi_{ij}(\mathbf{q}, i\nu_n) = -\int_0^\beta d\tau e^{i\nu_n\tau}\langle T_\tau\{\rho_{i\boldsymbol{q}}(\tau)\rho_{j-\boldsymbol{q}}(0)\}\rangle$$

$$= \frac{1}{\beta}\sum_{\boldsymbol{p},\omega_m} \mathrm{Tr}\left[\tau_i\hat{G}\left(\mathbf{p} + \frac{\mathbf{q}}{2}, i\omega_m + i\nu_n\right)\right.$$

$$\left.\times\,\tau_j\hat{G}\left(\mathbf{p} - \frac{\mathbf{q}}{2}, i\omega_m\right)\right], \tag{3.19}$$

where the second line ($\equiv \Pi^0_{ij}$) is the approximation neglecting the effect of the interactions $-U$ and g_{r}.

Equation (3.19) also defines other correlation functions, which will be important, such as Π_{11} and Π_{12}. Physically, Π_{11} and Π_{22} describe, respectively, the amplitude and phase fluctuations of Cooper pairs. Π_{33} describes density fluctuations in the gas of Fermi atoms. Π_{ij} with $i\neq j$ describes a coupling between fluctuations, e.g., Π_{12} is a coupling of amplitude fluctuations with the phase fluctuations (amplitude-phase coupling).

Summing up the Matsubara frequencies in Eq. (3.19), we obtain [35,40]

$$\Pi_{11}^0=\sum_{\boldsymbol{p}}\left(1-\frac{\xi_{\boldsymbol{p}+\boldsymbol{q}/2}\xi_{\boldsymbol{p}-\boldsymbol{q}/2}-\tilde{\Delta}^2}{E_{\boldsymbol{p}+\boldsymbol{q}/2}E_{\boldsymbol{p}-\boldsymbol{q}/2}}\right)\frac{E_{\boldsymbol{p}+\boldsymbol{q}/2}-E_{\boldsymbol{p}-\boldsymbol{q}/2}}{(E_{\boldsymbol{p}+\boldsymbol{q}/2}-E_{\boldsymbol{p}-\boldsymbol{q}/2})^2+\nu_n^2}\times[f(E_{\boldsymbol{p}+\boldsymbol{q}/2})-f(E_{\boldsymbol{p}-\boldsymbol{q}/2})]-\sum_{\boldsymbol{p}}\left(1+\frac{\xi_{\boldsymbol{p}+\boldsymbol{q}/2}\xi_{\boldsymbol{p}-\boldsymbol{q}/2}-\tilde{\Delta}^2}{E_{\boldsymbol{p}+\boldsymbol{q}/2}E_{\boldsymbol{p}-\boldsymbol{q}/2}}\right)\frac{E_{\boldsymbol{p}+\boldsymbol{q}/2}+E_{\boldsymbol{p}-\boldsymbol{q}/2}}{(E_{\boldsymbol{p}+\boldsymbol{q}/2}+E_{\boldsymbol{p}-\boldsymbol{q}/2})^2+\nu_n^2}\times[1-f(E_{\boldsymbol{p}+\boldsymbol{q}/2})-f(E_{\boldsymbol{p}-\boldsymbol{q}/2})], \tag{3.20}$$

$$\Pi_{22}^0=\sum_{\boldsymbol{p}}\left(1-\frac{\xi_{\boldsymbol{p}+\boldsymbol{q}/2}\xi_{\boldsymbol{p}-\boldsymbol{q}/2}+\tilde{\Delta}^2}{E_{\boldsymbol{p}+\boldsymbol{q}/2}E_{\boldsymbol{p}-\boldsymbol{q}/2}}\right)\frac{E_{\boldsymbol{p}+\boldsymbol{q}/2}-E_{\boldsymbol{p}-\boldsymbol{q}/2}}{(E_{\boldsymbol{p}+\boldsymbol{q}/2}-E_{\boldsymbol{p}-\boldsymbol{q}/2})^2+\nu_n^2}\times[f(E_{\boldsymbol{p}+\boldsymbol{q}/2})-f(E_{\boldsymbol{p}-\boldsymbol{q}/2})]-\sum_{\boldsymbol{p}}\left(1+\frac{\xi_{\boldsymbol{p}+\boldsymbol{q}/2}\xi_{\boldsymbol{p}-\boldsymbol{q}/2}+\tilde{\Delta}^2}{E_{\boldsymbol{p}+\boldsymbol{q}/2}E_{\boldsymbol{p}-\boldsymbol{q}/2}}\right)\frac{E_{\boldsymbol{p}+\boldsymbol{q}/2}+E_{\boldsymbol{p}-\boldsymbol{q}/2}}{(E_{\boldsymbol{p}+\boldsymbol{q}/2}+E_{\boldsymbol{p}-\boldsymbol{q}/2})^2+\nu_n^2}\times[1-f(E_{\boldsymbol{p}+\boldsymbol{q}/2})-f(E_{\boldsymbol{p}-\boldsymbol{q}/2})], \tag{3.21}$$

$$\Pi_{33}^0=\sum_{\boldsymbol{p}}\left(1+\frac{\xi_{\boldsymbol{p}+\boldsymbol{q}/2}\xi_{\boldsymbol{p}-\boldsymbol{q}/2}-\tilde{\Delta}^2}{E_{\boldsymbol{p}+\boldsymbol{q}/2}E_{\boldsymbol{p}-\frac{\boldsymbol{q}}{2}}}\right)\frac{E_{\boldsymbol{p}+\boldsymbol{q}/2}-E_{\boldsymbol{p}-\boldsymbol{q}/2}}{(E_{\boldsymbol{p}+\boldsymbol{q}/2}-E_{\boldsymbol{p}-\boldsymbol{q}/2})^2+\nu_n^2}\times[f(E_{\boldsymbol{p}+\boldsymbol{q}/2})-f(E_{\boldsymbol{p}-\boldsymbol{q}/2})]-\sum_{\boldsymbol{p}}\left(1-\frac{\xi_{\boldsymbol{p}+\boldsymbol{q}/2}\xi_{\boldsymbol{p}-\boldsymbol{q}/2}-\tilde{\Delta}^2}{E_{\boldsymbol{p}+\boldsymbol{q}/2}E_{\boldsymbol{p}-\boldsymbol{q}/2}}\right)\times\frac{E_{\boldsymbol{p}+\boldsymbol{q}/2}+E_{\boldsymbol{p}-\boldsymbol{q}/2}}{(E_{\boldsymbol{p}+\boldsymbol{q}/2}+E_{\boldsymbol{p}-\boldsymbol{q}/2})^2+\nu_n^2}[1-f(E_{\boldsymbol{p}+\boldsymbol{q}/2})-f(E_{\boldsymbol{p}-\boldsymbol{q}/2})]. \tag{3.22}$$

The correlation functions Π_{ij}^0 $(i\neq j)$ describing the coupling of different operators are given by

$$\Pi_{12}^0=\sum_{\boldsymbol{p}}\left(\frac{\xi_{\boldsymbol{p}+\boldsymbol{q}/2}}{E_{\boldsymbol{p}+\boldsymbol{q}/2}}-\frac{\xi_{\boldsymbol{p}-\boldsymbol{q}/2}}{E_{\boldsymbol{p}-\boldsymbol{q}/2}}\right)\frac{\nu_n}{(E_{\boldsymbol{p}+\boldsymbol{q}/2}-E_{\boldsymbol{p}-\boldsymbol{q}/2})^2+\nu_n^2}\times[f(E_{\boldsymbol{p}+\boldsymbol{q}/2})-f(E_{\boldsymbol{p}-\boldsymbol{q}/2})]-\sum_{\boldsymbol{p}}\left(\frac{\xi_{\boldsymbol{p}+\boldsymbol{q}/2}}{E_{\boldsymbol{p}+\boldsymbol{q}/2}}+\frac{\xi_{\boldsymbol{p}-\boldsymbol{q}/2}}{E_{\boldsymbol{p}-\boldsymbol{q}/2}}\right)\frac{\nu_n}{(E_{\boldsymbol{p}+\boldsymbol{q}/2}+E_{\boldsymbol{p}-\boldsymbol{q}/2})^2+\nu_n^2}\times[1-f(E_{\boldsymbol{p}+\boldsymbol{q}/2})-f(E_{\boldsymbol{p}-\boldsymbol{q}/2})], \tag{3.23}$$

$$\Pi_{23}^0=-\tilde{\Delta}\,\nu_n\sum_{\boldsymbol{p}}\left(\frac{1}{E_{\boldsymbol{p}+\boldsymbol{q}/2}}-\frac{1}{E_{\boldsymbol{p}-\boldsymbol{q}/2}}\right)\frac{1}{(E_{\boldsymbol{p}+\boldsymbol{q}/2}-E_{\boldsymbol{p}-\boldsymbol{q}/2})^2+\nu_n^2}\times[f(E_{\boldsymbol{p}+\boldsymbol{q}/2})-f(E_{\boldsymbol{p}-\boldsymbol{q}/2})]+\tilde{\Delta}\,\nu_n\sum_{\boldsymbol{p}}\left(\frac{1}{E_{\boldsymbol{p}+\boldsymbol{q}/2}}+\frac{1}{E_{\boldsymbol{p}-\boldsymbol{q}/2}}\right)\frac{1}{(E_{\boldsymbol{p}+\boldsymbol{q}/2}+E_{\boldsymbol{p}-\boldsymbol{q}/2})^2+\nu_n^2}\times[1-f(E_{\boldsymbol{p}+\boldsymbol{q}/2})-f(E_{\boldsymbol{p}-\boldsymbol{q}/2})], \tag{3.24}$$

$$\Pi_{13}^0=-\tilde{\Delta}\sum_{\boldsymbol{p}}\frac{\xi_{\boldsymbol{p}+\boldsymbol{q}/2}+\xi_{\boldsymbol{p}-\boldsymbol{q}/2}}{E_{\boldsymbol{p}+\boldsymbol{q}/2}E_{\boldsymbol{p}-\boldsymbol{q}/2}}\frac{E_{\boldsymbol{p}+\boldsymbol{q}/2}-E_{\boldsymbol{p}-\boldsymbol{q}/2}}{(E_{\boldsymbol{p}+\boldsymbol{q}/2}-E_{\boldsymbol{p}-\boldsymbol{q}/2})^2+\nu_n^2}\times[f(E_{\boldsymbol{p}+\boldsymbol{q}/2})-f(E_{\boldsymbol{p}-\boldsymbol{q}/2})]-\tilde{\Delta}\sum_{\boldsymbol{p}}\frac{\xi_{\boldsymbol{p}+\boldsymbol{q}/2}+\xi_{\boldsymbol{p}-\boldsymbol{q}/2}}{E_{\boldsymbol{p}+\boldsymbol{q}/2}E_{\boldsymbol{p}-\boldsymbol{q}/2}}\frac{E_{\boldsymbol{p}+\boldsymbol{q}/2}+E_{\boldsymbol{p}-\boldsymbol{q}/2}}{(E_{\boldsymbol{p}+\boldsymbol{q}/2}+E_{\boldsymbol{p}-\boldsymbol{q}/2})^2+\nu_n^2}\times[1-f(E_{\boldsymbol{p}+\boldsymbol{q}/2})-f(E_{\boldsymbol{p}-\boldsymbol{q}/2})], \tag{3.25}$$

with $\Pi_{21}^0=-\Pi_{12}^0$, $\Pi_{32}^0=-\Pi_{23}^0$, and $\Pi_{31}^0=\Pi_{13}^0$. The density-density correlation function Π_{33}^0 and the related coupling correlation functions Π_{13}^0 and Π_{23}^0 will be used in Sec. VI, where we show that the Goldstone mode describing the collective phase oscillation of Cooper pairs has spectral weight in the density correlation function. This weight comes from the coupling to the amplitude-density (Π_{13}^0) and phase-density (Π_{23}^0) correlation.

The factor $E_{\boldsymbol{p}+\boldsymbol{q}/2}-E_{\boldsymbol{p}-\boldsymbol{q}/2}$ in the denominator of the first line in Eqs. (3.20)–(3.25) describes scattering between excitations with momenta $\mathbf{p}\pm\mathbf{q}/2$ in the *same* quasiparticle band $E_{\boldsymbol{p}}$. For this reason, the first line in Eqs. (3.20)–(3.25) is referred to as the *intraband* term [35]. Since the thermal excitations of fermion quasi-particles are absent at $T=0$, the intraband term vanishes at $T=0$. On the other hand, the second line in Eqs. (3.20)–(3.25) is finite even at $T=0$. The factor $E_{\boldsymbol{p}+\boldsymbol{q}/2}+E_{\boldsymbol{p}-\boldsymbol{q}/2}$ in the denominator describes *interband* scattering between $E_{\boldsymbol{p}+\boldsymbol{q}/2}$ and $-E_{\boldsymbol{p}-\boldsymbol{q}/2}$, and thus the second line in Eqs. (3.20)–(3.25) is called the *interband* term. The intraband term is known to give rise to Landau damping of collective modes *below* the excitation gap $2\tilde{\Delta}$, while the damping due to the interband term only exists *above* $2\tilde{\Delta}$ [35]. We note that the gap equation in Eq. (3.16) can be neatly expressed in terms of Π_{22}^0 in Eq. (3.21), namely,

$$1+\frac{U_{\mathrm{eff}}}{2}\Pi_{22}^0(0,0)=0. \tag{3.26}$$

The fluctuation contribution $\delta\Omega_1$ involving the amplitude fluctuations of Cooper pairs is similarly obtained by summing up the loop-type diagrams in Fig. 4(a) associated with the amplitude-amplitude interaction $-(U/4)\Sigma_{\boldsymbol{q}}\rho_{1\boldsymbol{q}}\rho_{1-\boldsymbol{q}}$. This gives

$$\delta\Omega_1=\frac{1}{2\beta}\sum_{\boldsymbol{q},\nu_n}\ln\left[1+\frac{U}{2}\Pi_{11}^0(\mathbf{q},i\nu_n)\right]. \tag{3.27}$$

The phase and amplitude fluctuations are coupled with each other through the amplitude-phase coupling Π_{12}^0 in Eq. (3.23). This additional coupling effect can be formally incorporated into $\delta\Omega_1$ by replacing $\Pi_{11}^0(\mathbf{q},i\nu_n)$ in Eq. (3.27) by $\overline{\Pi}_{11}(\mathbf{q},i\nu_n)$, where

$$\overline{\Pi}_{11}(\mathbf{q},i\nu_n)\equiv\Pi_{11}^0(\mathbf{q},i\nu_n)+\Pi_{12}^0(\mathbf{q},i\nu_n)\times\frac{-U/2}{1+(U/2)\Pi_{22}^0(\mathbf{q},i\nu_n)}\Pi_{21}^0(\mathbf{q},i\nu_n). \tag{3.28}$$

The second term describes the amplitude-phase coupling effect through the coupling correlation functions Π_{12}^0 and Π_{21}^0. Equation (3.28) is obtained by summing up the fluctuation diagrams shown in Fig. 4(b).

In summary, the fluctuation contribution $\delta\Omega_U$ to the thermodynamic potential involving only the nonresonant interaction $-U$ is the sum of Eqs. (3.18) and (3.28) with $\Pi_{11}^0 \to \overline{\Pi}_{11}$. The sum is given by

$$\begin{aligned}\delta\Omega_U&=\frac{1}{2\beta}\sum_{\mathbf{q},\nu_n}\ln\left(\left[1+\frac{U}{2}\overline{\Pi}_{11}(\mathbf{q},i\nu_n)\right]\left[1+\frac{U}{2}\Pi_{22}^0(\mathbf{q},i\nu_n)\right]\right)\\&=\frac{1}{2\beta}\sum_{\mathbf{q},\nu_n}\ln\left(\left[1+\frac{U}{2}\Pi_{11}^0(\mathbf{q},i\nu_n)\right]\left[1+\frac{U}{2}\Pi_{22}^0(\mathbf{q},i\nu_n)\right]-\left(\frac{U}{2}\right)^2\Pi_{12}^0(\mathbf{q},i\nu_n)\Pi_{21}^0(\mathbf{q},i\nu_n)\right)\\&=\frac{1}{2\beta}\sum_{\mathbf{q},\nu_n}\ln\det\left[1+\frac{U}{2}\hat{\Pi}^0(\mathbf{q},i\nu_n)\right]\\&=\frac{1}{2\beta}\sum_{\mathbf{q},\nu_n}\mathrm{Tr}\ln\left[1+\frac{U}{2}\hat{\Pi}^0(\mathbf{q},i\nu_n)\right],\end{aligned} \tag{3.29}$$

where we have used the well-known identity $\det\hat{A}=e^{\mathrm{Tr}[\ln\hat{A}]}$ in the last expression. $\hat{\Pi}^0(\mathbf{q},i\nu_n)$ is a 2×2-matrix density correlation function, defined by

$$\hat{\Pi}^0(\mathbf{q},i\nu_n)=\begin{pmatrix}\Pi_{11}^0 & \Pi_{12}^0\\ \Pi_{21}^0 & \Pi_{22}^0\end{pmatrix}. \tag{3.30}$$

Finally, we consider the fluctuation contributions $\delta\Omega_{\mathrm{FR}}$ from the Feshbach resonance term $\frac{1}{2}g_r\Sigma_{\mathbf{q}}[b_{\mathbf{q}}^\dagger\rho_{\mathbf{q}}^- + b_{\mathbf{q}}\rho_{\mathbf{q}}^+]$ in Eq. (3.7). First we sum up the diagrams described in Fig. 4(a), where the dashed line now represents the *b*-boson Green's function $D_0(\mathbf{q},i\nu_n)$ in Eq. (3.4), to give

$$\delta\Omega_{\mathrm{FR}}=\frac{1}{2\beta}\sum_{\mathbf{q},\nu_n}\mathrm{Tr}\ln\left[1-\frac{g_r^2}{4}\hat{D}^0(\mathbf{q},i\nu_n)\hat{\Xi}^0(\mathbf{q},i\nu_n)\right]. \tag{3.31}$$

Here, $\hat{D}^0(\mathbf{q},i\nu_n)$ is a 2×2-matrix *b*-boson Green's function defined by

$$\hat{D}^0(\mathbf{q},\nu_n)=\frac{1}{i\nu_n\tau_3-\xi_{B\mathbf{q}}}=-\frac{i\nu_n\tau_3+\xi_{B\mathbf{q}}}{\nu_n^2+\xi_{B\mathbf{q}}^2}, \tag{3.32}$$

and $\hat{\Xi}^0(\mathbf{q},i\nu_n)$ is a 2×2-matrix correlation function (neglecting the effect of $-U$ and g_r) defined by

$$\hat{\Xi}^0(\mathbf{q},i\nu_n)=-\int_0^\beta d\tau e^{i\nu_n\tau}\times\left\langle T_\tau\left[\begin{pmatrix}\rho_{\mathbf{q}}^-(\tau)\rho_{-\mathbf{q}}^+(0) & \rho_{\mathbf{q}}^-(\tau)\rho_{-\mathbf{q}}^-(0)\\ \rho_{\mathbf{q}}^+(\tau)\rho_{-\mathbf{q}}^+(0) & \rho_{\mathbf{q}}^+(\tau)\rho_{-\mathbf{q}}^-(0)\end{pmatrix}\right]\right\rangle. \tag{3.33}$$

Using the definition $\rho_{\mathbf{q}}^\pm=\rho_{1\pm\mathbf{q}}\pm i\rho_{2\pm\mathbf{q}}$, we find that $\hat{\Xi}^0$ can be expressed in terms of the matrix elements of $\hat{\Pi}^0$ as follows:

$$\begin{aligned}\hat{\Xi}^0&=2\hat{W}^{-1}\hat{\Pi}^0\hat{W}\\&=\begin{pmatrix}\Pi_{11}^0+\Pi_{22}^0+i(\Pi_{12}^0-\Pi_{21}^0) & \Pi_{11}^0-\Pi_{22}^0\\ \Pi_{11}^0-\Pi_{22}^0 & \Pi_{11}^0+\Pi_{22}^0-i(\Pi_{12}^0-\Pi_{21}^0)\end{pmatrix},\end{aligned} \tag{3.34}$$

where $\hat{W}$ is the unitary matrix

$$\hat{W}=\frac{1}{\sqrt{2}}\begin{pmatrix}1 & 1\\ i & -i\end{pmatrix}. \tag{3.35}$$

Next we renormalize the fluctuations in Eq. (3.31) by including the effects of the nonresonant interaction $-U$ on the correlation function $\hat{\Xi}^0(\mathbf{q},i\nu_n)$, working within the HF-RPA. This results in $\hat{\Xi}^0(\mathbf{q},i\nu_n)$ in Eq. (3.31) being replaced by $\hat{\Xi}_U$, where [35,36]

$$\hat{\Xi}_U(\mathbf{q},i\nu_n)=\left[1+\frac{U}{4}\hat{\Xi}^0(\mathbf{q},i\nu_n)\right]^{-1}\hat{\Xi}^0(\mathbf{q},i\nu_n). \tag{3.36}$$

The resulting expression for $\delta\Omega_{\mathrm{FR}}$ involves the fluctuation effects related to both the nonresonant interaction $-U$ and the Feshbach resonance coupling parameter g_r, namely,

$$\begin{aligned}\delta\Omega_{\mathrm{FR}}&=\frac{1}{2\beta}\sum_{\mathbf{q},\nu_n}\mathrm{Tr}\ln\left[1-\frac{g_r^2}{4}\hat{D}^0(\mathbf{q},i\nu_n)\hat{\Xi}_U(\mathbf{q},i\nu_n)\right]\\&=\frac{1}{2\beta}\sum_{\mathbf{q},\nu_n}\mathrm{Tr}\ln\left\{1-\frac{g_r^2}{4}\hat{D}^0(\mathbf{q},i\nu_n)\times\left[1+\frac{U}{4}\hat{\Xi}^0(\mathbf{q},i\nu_n)\right]^{-1}\hat{\Xi}^0(\mathbf{q},i\nu_n)\right\}.\end{aligned} \tag{3.37}$$

The total fluctuation contribution $\delta\Omega$ is given by the sum of Eqs. (3.29) and (3.37). Recalling the definition in Eq. (3.34) and the relation $\mathrm{Tr}\ln[1+(U/2)\hat{\Pi}^0]=\mathrm{Tr}\ln[\hat{W}\{1+(U/4)\hat{\Xi}^0\}\hat{W}^{-1}]=\mathrm{Tr}\ln[1+(U/4)\hat{\Xi}^0]$, this sum can be written as

$$\delta\Omega \equiv \delta\Omega_U + \delta\Omega_{\rm FR} = \frac{1}{2\beta}\sum_{\mathbf{q},\nu_n} {\rm Tr}\ln\left\{1+\frac{1}{4}[U-g_{\rm r}^2\hat{D}^0(\mathbf{q},i\nu_n)]\hat{\Xi}^0(\mathbf{q},i\nu_n)\right\}. \tag{3.38}$$

Putting everything together, the total thermodynamic potential $\Omega=\Omega_{\rm MF}+\delta\Omega$ is

$$\Omega = \frac{\tilde{\Delta}^2}{U_{\rm eff}} + \sum_{\mathbf{p}} (\xi_{\mathbf{p}} - E_{\mathbf{p}}) - 2T\sum_{\mathbf{p}} \ln[1+e^{-\beta E_{\mathbf{p}}}] + T\sum_{\mathbf{q}} \ln[1-e^{-\beta\xi^B_{\mathbf{q}}}] + \frac{1}{2\beta} \times \sum_{\mathbf{q},\nu_n} {\rm Tr}\ln\left\{1+\frac{1}{4}[U-g_{\rm r}^2\hat{D}^0(\mathbf{q},i\nu_n)]\hat{\Xi}^0(\mathbf{q},i\nu_n)\right\}. \tag{3.39}$$

The equation for the total number of particles is then obtained from $N=-\partial\Omega/\partial\mu$.

In taking the derivative with respect to μ, we note that the order parameter $\tilde{\Delta}$ also depends on the chemical potential μ, in addition to $\xi_{\mathbf{p}}\equiv\varepsilon_{\mathbf{p}}-\mu$ and $\xi_{B\mathbf{q}}\equiv\varepsilon_{B\mathbf{q}}+2\nu-2\mu$. Thus, one needs to calculate

$$\frac{\partial\Omega}{\partial\tilde{\Delta}}\frac{\partial\tilde{\Delta}}{\partial\mu} = \frac{\partial\Omega_{\rm MF}}{\partial\tilde{\Delta}}\frac{\partial\tilde{\Delta}}{\partial\mu} + \frac{\partial\delta\Omega}{\partial\tilde{\Delta}}\frac{\partial\tilde{\Delta}}{\partial\mu} = \frac{\partial\delta\Omega}{\partial\tilde{\Delta}}\frac{\partial\tilde{\Delta}}{\partial\mu}. \tag{3.40}$$

In the last line, we have used the fact $\partial\Omega_{\rm MF}/\partial\tilde{\Delta}=0$, which holds when $\tilde{\Delta}$ satisfies the gap equation (3.16). However, one can show that $\partial\delta\Omega/\partial\tilde{\Delta}$ in Eq. (3.40) is a higher-order correction within the perturbative approximation we are using [41], so that we can neglect the contribution in Eq. (3.40). Thus, the dependence of $\tilde{\Delta}$ on μ only leads to higher-order corrections. The resulting equation for N is

$$N = 2\phi_{\rm m}^2 + \sum_{\mathbf{p}}\left[1-\frac{\xi_{\mathbf{p}}}{E_{\mathbf{p}}}\tanh\frac{\beta}{2}E_{\mathbf{p}}\right] + 2\sum_{\mathbf{q}} n_{\rm B}(\xi^B_{\mathbf{q}}) - \frac{1}{2\beta}\sum_{\mathbf{q},\nu_n}\frac{\partial}{\partial\mu}{\rm Tr}\ln\left\{1+\frac{1}{4}[U-g_{\rm r}^2\hat{D}^0(\mathbf{q},i\nu_n)] \times\hat{\Xi}^0(\mathbf{q},i\nu_n)\right\}. \tag{3.41}$$

Here, it is understood that the μ derivative in the last term only acts on the chemical potential involved in $\xi_{\mathbf{p}}$ and $\xi_{B\mathbf{q}}$. Equations (3.16) and (3.41) give us the required self-consistent coupled equations for $\tilde{\Delta}$ and μ in the superfluid phase below $T_{\rm c}$. We will discuss our numerical self-consistent solutions of the coupled equations (3.16) and (3.41) in Sec. V.

When one neglects the fluctuation contribution given in the last term in Eq. (3.41), we obtain the mean-field expression obtained in Ref. [24] in the context of high-$T_{\rm c}$ superconductivity. We also mention that Eq. (3.41) reproduces Eq. (3.3) for the normal phase $T\geqslant T_{\rm c}$, where $\Delta=\phi_{\rm m}=0$. To see this, we note that the second term on the right-hand side in Eq. (3.41) reduces to $2N_{\rm F}^0$ in Eq. (3.3). In addition, since the phase and amplitude fluctuations are indistinguishable when $\Delta=0$, we find $\Pi^0_{11}=\Pi^0_{22}$, and thus $\hat{\Xi}_0$ in Eq. (3.34) becomes diagonal at $T_{\rm c}$. Noting that $\Xi^0_{11}(\mathbf{q},i\nu_n,T=T_{\rm c})=-4\Pi(\mathbf{q},i\nu_n)$ and $\Xi^0_{22}(\mathbf{q},i\nu_n,T=T_{\rm c})=-4\Pi(\mathbf{q},-i\nu_n)$, where $\Pi(\mathbf{q},i\nu_n)$ is given in Eq. (3.5), we find that the last term in Eq. (3.41) ($\equiv\delta N$) reproduces the last term in Eq. (3.3). More explicitly, we have

$$\begin{aligned}\delta N(T_{\rm c}) &= -\frac{1}{2\beta}\sum_{\mathbf{q},\nu_n}\frac{\partial}{\partial\mu}\ln[\{1-[U-g_{\rm r}^2D^0_{11}(\mathbf{q},i\nu_n)] \times\Pi(\mathbf{q},i\nu_n)\}\{1-[U-g_{\rm r}^2D^0_{22}(\mathbf{q},i\nu_n)] \times\Pi(\mathbf{q},-i\nu_n)\}] \\ &= -\frac{1}{\beta}\sum_{\mathbf{q},\nu_n}\frac{\partial}{\partial\mu}\ln\{1-[U-g_{\rm r}^2D_0(\mathbf{q},i\nu_n)]\Pi(\mathbf{q},i\nu_n)\},\end{aligned} \tag{3.42}$$

where we have used $D^0_{11}(\mathbf{q},i\nu_n)=D_0(\mathbf{q},i\nu_n)$ and $D^0_{22}(\mathbf{q},i\nu_n)=D_0(\mathbf{q},-i\nu_n)$ in the last line. Thus, Eq. (3.41) is equivalent to Eq. (3.3) at $T_{\rm c}$. Our present strong-coupling theory giving the coupled equations (3.16) and (3.41) for the superfluid phase is seen to smoothly go over to our previous discussion at $T_{\rm c}$ and above [12–14].

Each term in Eq. (3.41) has a simple physical meaning, which is useful to discuss. The first term

$$2N_{\rm B}^{\rm c}\equiv 2\phi_{\rm m}^2 = 2\langle b_{\mathbf{q}=0}\rangle^2 \tag{3.43}$$

gives twice the number of Bose-*condensed* b bosons. The second term

$$N_{\rm F}\equiv\sum_{\mathbf{p}}\left[1-\frac{\xi_{\mathbf{p}}}{E_{\mathbf{p}}}\tanh\frac{\beta}{2}E_{\mathbf{p}}\right] \tag{3.44}$$

describes the number of Fermi quasiparticles. This expression can be directly obtained from $N_{\rm F}=\Sigma_{\mathbf{p},\sigma}\langle c^\dagger_{\mathbf{p}\sigma}c_{\mathbf{p}\sigma}\rangle$ in Eq. (2.2). To understand the physical meanings of the last two terms in Eq. (3.41), it is convenient to divide the μ derivative in the last term into the derivative acting on $\xi_{B\mathbf{q}}=q^2/2M+2\nu-2\mu$ in the b-boson Green's function $\hat{D}^0(\mathbf{q},i\nu_n)$ and the derivative acting on $\xi_{\mathbf{p}}=\varepsilon_{\mathbf{p}}-\mu$ in $\Xi^0(\mathbf{q},i\nu_n)$ ($\equiv\partial/\partial\mu_{\rm F}$). Using the identity

$$2\sum_{\mathbf{q}} n_{\rm B}(\xi_{B\mathbf{q}}) = -\sum_{\mathbf{q}}\left[1+\frac{1}{\beta}\sum_{\nu_n}{\rm Tr}[\hat{D}^0(\mathbf{q},i\nu_n)]\right], \tag{3.45}$$

we can write Eq. (3.41) as

$$N = 2N_{\rm B}^{\rm c} + N_{\rm F} + 2N_{\rm B}^{\rm n} + 2N_{\rm C}, \tag{3.46}$$

where $N_{\rm B}^{\rm n}$ and $N_{\rm C}$ are defined by

$$2N_{\rm B}^{\rm n} \equiv -\sum_{\mathbf{q}} \left[1+\frac{1}{\beta}\sum_{\nu_n} {\rm Tr}[\hat{D}(\mathbf{q},i\nu_n)] \right],$$

$$2N_{\rm C} \equiv -\frac{1}{2\beta}\sum_{\mathbf{q},\nu_n}\frac{\partial}{\partial\mu_{\rm F}}{\rm Tr}\ln\left\{ 1+\frac{1}{4}[U-g_{\rm r}^2\hat{D}^0(\mathbf{q},i\nu_n)] \times\hat{\Xi}^0(\mathbf{q},i\nu_n)\right\}. \quad (3.47)$$

Here, $\hat{D}(\mathbf{q},i\nu_n)$ is a renormalized 2×2-matrix thermal b-boson Green's function defined by

$$\hat{D}(\mathbf{q},i\nu_n)=\frac{1}{i\nu_n\tau_3-\xi_{B\mathbf{q}}-\hat{\Sigma}(\mathbf{q},i\nu_n)}. \quad (3.48)$$

The b-boson matrix self-energy

$$\hat{\Sigma}(\mathbf{q},i\nu_n)\equiv\frac{g_{\rm r}^2}{4}\hat{\Xi}_U(\mathbf{q},i\nu_n) =\frac{g_{\rm r}^2}{4}\left[1+\frac{U}{4}\hat{\Xi}^0(\mathbf{q},i\nu_n)\right]^{-1}\hat{\Xi}^0(\mathbf{q},i\nu_n) \quad (3.49)$$

describes the Feshbach coupling with Fermi atoms.

The renormalized b-boson Green's function in Eq. (3.48) has the same form as that obtained by Kostyrko and Ranninger [24] calculated within the HF-RPA. Comparing $N_{\rm B}^{\rm n}$ in Eq. (3.47) with Eq. (3.45), we may interpret $N_{\rm B}^{\rm n}$ as the number of *noncondensed b* bosons, as renormalized by the Feshbach resonance. In analogy to our previous discussion of the strong-coupling theory for $T_{\rm c}$ [12–14], $N_{\rm C}$ in Eq. (3.47) may be understood as the fluctuation contribution to N from Cooper pairs associated with the (dynamical) pairing interaction given by

$$\hat{U}_{\rm eff}(\mathbf{q},i\nu_n)\equiv U-g_{\rm r}^2\hat{D}^0(\mathbf{q},i\nu_n). \quad (3.50)$$

We note that $\hat{U}_{\rm eff}(\mathbf{q}=0,i\nu_n=0)=U_{\rm eff}\hat{\mathbf{1}}$, where $U_{\rm eff}=U+g_{\rm r}^2/(2\nu-2\mu)$ is the effective pairing interaction appearing in the gap equation in Eq. (3.16).

The renormalized b-boson Green's function in Eq. (3.48) can be also written in the form

$$\hat{D}(\mathbf{q},i\nu_n)=\frac{1}{i\tilde{\nu}_n\tau_3-\tilde{\xi}_{B\mathbf{q}}-\kappa\tau_1}=-\frac{i\tilde{\nu}_n\tau_3+\tilde{\xi}_{B\mathbf{q}}-\kappa\tau_1}{\tilde{\nu}_n^2+\tilde{\xi}_{B\mathbf{q}}^2-\kappa^2}, \quad (3.51)$$

where the renormalized parameters are given by

$$i\tilde{\nu}_n\equiv i\nu_n-i\frac{g_{\rm r}^2}{4}[\Pi_{U12}-\Pi_{U21}],$$

$$\tilde{\xi}_{B\mathbf{q}}\equiv\xi_{B\mathbf{q}}+\frac{g_{\rm r}^2}{4}[\Pi_{U11}+\Pi_{U22}], \quad (3.52)$$

$$\kappa\equiv\frac{g_{\rm r}^2}{4}[\Pi_{U11}-\Pi_{U22}].$$

The correlation functions Π_{Uij} $(i,j=1,2)$ are the matrix elements of $\hat{\Pi}_U$ defined by

$$\hat{\Pi}_U(\mathbf{q},i\nu_n)=\left[1+\frac{U}{2}\hat{\Pi}^0(\mathbf{q},i\nu_n)\right]^{-1}\hat{\Pi}^0(\mathbf{q},i\nu_n). \quad (3.53)$$

More explicitly, we have

$$\Pi_{U11}=\frac{\overline{\Pi}_{11}}{1+\frac{U}{2}\overline{\Pi}_{11}},$$

$$\Pi_{U22}=\frac{\overline{\Pi}_{22}}{1+\frac{U}{2}\overline{\Pi}_{22}},$$

$$\Pi_{U12}=\frac{\Pi_{12}^0}{\left[1+\frac{U}{2}\Pi_{11}^0\right]\left[1+\frac{U}{2}\Pi_{22}^0\right]-\frac{U^2}{4}\Pi_{12}^0\Pi_{21}^0}, \quad (3.54)$$

$$\Pi_{U21}(\mathbf{q},i\nu_n)=-\Pi_{U12}(\mathbf{q},i\nu_n).$$

Here, $\overline{\Pi}_{11}$ is defined in Eq. (3.28) and $\overline{\Pi}_{22}$ is similarly obtained from Eq. (3.28) by interchanging $1\leftrightarrow2$.

When we take $\mathbf{q}=i\nu_n=0$, the denominator of Eq. (3.51) reduces to

$$\tilde{\xi}_{B\mathbf{q}=0}^2-\kappa(0,0)^2=\left[1+\frac{U_{\rm eff}}{2}\Pi_{22}^0(0,0)\right]\left[1+\frac{U_{\rm eff}}{2}\Pi_{11}^0(0,0)\right] \times\frac{2\nu-2\mu}{1+\frac{U}{2}\Pi_{22}^0(0,0)}\,\frac{2\nu-2\mu}{1+\frac{U}{2}\Pi_{11}^0(0,0)}. \quad (3.55)$$

The expression in Eq. (3.55) clearly vanishes when the gap equation in Eq. (3.26) is satisfied. This means that the excitation spectrum of the renormalized b bosons described by $\hat{D}$ is always *gapless* at $\mathbf{q}=0$ for $T<T_{\rm c}$. This is a desired result, because the Bose-condensation of b bosons characterized by $\phi_{\rm m}$ should be accompanied by the appearance of a Bogoliubov phonon (Goldstone) mode having a (uniform system) gapless dispersion. Thus, the strong-coupling theory presented in this section correctly includes a gapless spectrum for the symmetry breaking Goldstone mode. This result is not obtained if we use a static mean-field theory, neglecting the fluctuation contribution given by the last term of Eq. (3.41). Within such a mean-field theory, the b-boson excitation spectrum is given by $\varepsilon_{B\mathbf{q}}+2\nu-2\mu$, which always has a *finite excitation gap* at $\mathbf{q}=0$. This gap is given by $\delta E\equiv2\nu-2\mu=-g_{\rm r}^2/2\Pi_{U22}(0,0)>0$, assuming that the gap equa-

tion in Eq. (3.26) is satisfied. We note that $\Pi_{U22}(0,0)$ is defined in Eq. (3.54), with $\overline{\Pi}_{22}(0,0)=\Pi^0_{22}(0,0)$ since $\Pi^0_{12}(0,0)=0$.

The gapless behavior of the renormalized b boson can be also verified formally by noting that the Hugenholtz-Pines theorem is verified, namely [24,42–44],

$$\Sigma_{11}(0,0)-\Sigma_{12}(0,0)=\frac{g_r^2}{2}\frac{\Pi^0_{22}(0,0)}{1+\frac{U}{2}\Pi^0_{22}(0,0)}=2\mu-2\nu. \tag{3.56}$$

Here, we have used the gap equation given in Eq. (3.26).

In order to discuss the BCS-BEC crossover in the superfluid phase, one needs to solve the coupled equations (3.16) and (3.41) numerically. Results will be discussed in Sec. V. Here, we briefly discuss limiting cases that can be treated analytically.

When the threshold energy 2ν of the b-boson excitation spectrum is very large (BCS limit), $2\nu \gg 2\mu$ can be realized because the chemical potential μ is at most the order of ε_F. In this case, the Fermi atoms are dominant particles, while the effects of b molecules described by ϕ_m, $n_B(\xi_{Bq})$ and $\hat{D}^0$ in Eq. (3.41) can be neglected. In addition, since the last term in Eq. (3.41) is small when one is dealing with a weak nonresonant interaction $-U$, one can also drop this term. Thus, we see that Eq. (3.41) reduces to $N=N_F$ [where N_F is defined in Eq. (3.44)], which simply gives $\mu \simeq \varepsilon_F$ if $\varepsilon_F \gg T$. When this result is substituted into the gap equation in Eq. (3.16) with $U_{\rm eff}\to U$ and $\tilde{\Delta}\to\Delta$ (note that $2\nu \gg 2\mu$), one obtains the usual BCS gap equation for the Cooper-pair order parameter Δ.

In the opposite limit $2\nu \lesssim -2\varepsilon_F$ (BEC limit), since the b-boson branch has an energy lower than the two fermion band energy, most Fermi atoms will combine to form b molecules and hence the fermion correlation functions Π_{ij} becomes less important. Then the gap equation in Eq. (3.26) can be rewritten as [see also Eq. (3.56)]

$$2\mu=2\nu+\frac{g_r^2}{2}\frac{\Pi^0_{22}(0,0)}{1+\frac{U}{2}\Pi^0_{22}(0,0)}\to 2\nu. \tag{3.57}$$

This says that the chemical potential has the energy of the bottom of the b-boson excitation spectrum. Substituting $2\mu=2\nu$ into Eq. (3.41) with $\hat{\Xi}^0(\mathbf{q},i\nu_n)=0$, we obtain

$$\frac{N}{2}=\phi_m+\sum_{\mathbf{q}} n_B\left(\frac{q^2}{2M}\right). \tag{3.58}$$

This is just the equation for BEC in an noninteracting uniform Bose gas with $N/2$ bosons of mass M. Thus, the coupled equations (3.16) and (3.41) reproduce both the BCS phase and BEC phase for two limiting values of the Feshbach molecular resonance threshold 2ν.

We again remind the reader about the many-body approximation our whole discussion is based. As we noted after Eq. (3.16), we have included the fluctuations of the order parameters Δ and ϕ_m in determining self-consistently the values of N and μ. However, we have not included the explicit self-energy of the fermions due to these dynamic fluctuations. For further discussion, see Refs. [38,34].

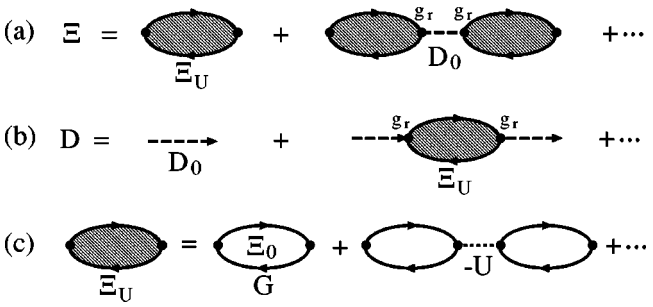

FIG. 5. The correlation function $\hat{\Xi}(\mathbf{q},i\nu_n)$ is shown in (a) and b-boson Green's function $\hat{D}(\mathbf{q},i\nu_n)$ is shown in (b), both within the HF-RPA. The shaded bubble $\hat{\Xi}_U(\mathbf{q},i\nu_n)$ shown in (c) includes RPA-type diagrams involving the nonresonant attractive interaction $-U$.

We note that the diagrammatic approach we have used in this section can be shown to be equivalent to keeping *Gaussian fluctuations* around the mean-field order parameters Δ and ϕ_m. Using the functional-integral formalism, which describes such fluctuations in a very clear fashion, Randeria and coworkers [20,45] showed that the strong-coupling superconductivity theory at T_c developed by Nozières and Schmitt-Rink [18] can be understood as a Gaussian approximation for the fluctuations in the Cooper channel. When we extend this kind of formalism to the coupled fermion-boson model in Eq. (2.1) below T_c, one finds the coupled equations (3.16) and (3.41) [41]. Recently, Milstein *et al.* [15] also employed this approach to the coupled fermion-boson model in Eq. (2.1) and obtained the equations for T_c given in Eqs. (3.1) and (3.3).

IV. GOLDSTONE MODES IN THE BCS-BEC CROSSOVER REGION

A. Correlation function and b-boson Green's function in the HF-RPA

The Goldstone mode in fermion superfluidity (Anderson-Bogoliubov) is a collective phase oscillation (phason) of Cooper pairs, and thus it appears as a pole in the phase correlation function $\Pi_{22}(\mathbf{q},i\nu_n\to\omega+i\delta)$. In the present coupled fermion-boson model, we also expect a Bogoliubov phonon mode associated with the BEC of b molecules characterized by the Bose order parameter $\phi_m=\langle b_{\mathbf{q}=0}\rangle$. This mode appears in the excitation spectrum of the b-boson Green's function $D(\mathbf{q},\tau)=-\langle T_\tau\{b_{\mathbf{q}}(\tau)b^\dagger_{\mathbf{q}}(0)\}\rangle$. However, since the Cooper-pair amplitude Δ and the b-boson order parameter ϕ_m are coupled with each other via the Feshbach resonance [see Eq. (2.5)], these two Goldstone modes are strongly hybridized.

In calculating the Goldstone mode, we have to be careful to use a consistent approximation for the self-energy and vertex correction. In this regard, apart from the chemical

potential, we recall that the gap equation in Eq. (3.16) is obtained from the Hartree-Fock Green's function in Eq. (3.11). Thus, we should employ the HF-RPA formalism for the correlation functions $\hat{\Pi}=\{\Pi_{ij}\}$ and b-boson Green's function [24,35,36]. Using the HF-RPA guarantees the gapless behavior of the Goldstone mode.

In calculating the correlation function $\hat{\Pi}$, it is convenient to first consider $\hat{\Xi}=2\hat{W}^{-1}\hat{\Pi}\hat{W}$ [see Eq. (3.34)]. Within the HF-RPA, $\hat{\Xi}$ is described by the sum of the diagrams in Fig. 5(a). The summation gives

$$\hat{\Xi}=\hat{\Xi}_U\left[1-\frac{1}{4}g_{\rm r}^2\hat{D}^0\hat{\Xi}_U\right]^{-1}=\hat{\Xi}^0\left[1+\frac{1}{4}[U-g_{\rm r}^2\hat{D}^0]\hat{\Xi}^0\right]^{-1}, \tag{4.1}$$

where $\hat{\Xi}_U$ involves the effect of nonresonant interaction $-U$ using the HF-RPA, as shown in Fig. 5(c) and given by Eq. (3.36). The correlation function $\hat{\Pi}$ is then obtained from the inverse relation $\hat{\Pi}=\frac{1}{2}\hat{W}\hat{\Xi}\hat{W}^{-1}$, namely,

$$\hat{\Pi}=\hat{\Pi}^0\left[1+\frac{1}{2}[U-g_{\rm r}^2\hat{W}\hat{D}^0\hat{W}^{-1}]\hat{\Pi}^0\right]^{-1}. \tag{4.2}$$

More explicitly, the amplitude and phase correlation functions Π_{11} and Π_{22} are given by

$$\Pi_{11}(\mathbf{q},i\nu_n)=\frac{\tilde{\Pi}_{11}}{1+\frac{V_1}{2}\tilde{\Pi}_{11}+\frac{V_2^2}{4}\frac{\Pi_{11}^0\Pi_{22}^0-\Pi_{12}^0\Pi_{21}^0}{1+\frac{V_1}{2}\Pi_{22}^0}-V_2\frac{\Pi_{12}^0}{1+\frac{V_1}{2}\Pi_{22}^0}},$$

$$\Pi_{22}(\mathbf{q},i\nu_n)=\frac{\tilde{\Pi}_{22}}{1+\frac{V_1}{2}\tilde{\Pi}_{22}+\frac{V_2^2}{4}\frac{\Pi_{11}^0\Pi_{22}^0-\Pi_{12}^0\Pi_{21}^0}{1+\frac{V_1}{2}\Pi_{11}^0}-V_2\frac{\Pi_{12}^0}{1+\frac{V_1}{2}\Pi_{11}^0}}, \tag{4.3}$$

where

$$\tilde{\Pi}_{11}\equiv\Pi_{11}^0+\Pi_{12}^0\frac{-\frac{V_1}{2}}{1+\frac{V_1}{2}\Pi_{22}^0}\Pi_{21}^0,$$

$$\tilde{\Pi}_{22}\equiv\Pi_{22}^0+\Pi_{21}^0\frac{-\frac{V_1}{2}}{1+\frac{V_1}{2}\Pi_{11}^0}\Pi_{12}^0, \tag{4.4}$$

$$V_1(\mathbf{q},i\nu_n)\equiv{\rm Re}[U_{\rm eff}(\mathbf{q},i\nu_n)]=U+g_{\rm r}^2\frac{\xi_{B\mathbf{q}}}{\nu_n^2+\xi_{B\mathbf{q}}^2},$$

$$V_2(\mathbf{q},i\nu_n)\equiv{\rm Im}[U_{\rm eff}(\mathbf{q},i\nu_n)]=g_{\rm r}^2\frac{\nu_n}{\nu_n^2+\xi_{B\mathbf{q}}^2}. \tag{4.5}$$

Here, the lowest-order noninteracting correlation functions Π_{ij}^0 are defined in Eqs. (3.20)–(3.25). V_1 describes amplitude-amplitude and phase-phase interactions, while V_2 is an amplitude-phase coupling mediated by b molecules. Since both V_2 and Π_{12}^0 vanish at $\mathbf{q}=i\nu_n=0$, the denominator of Π_{22} in Eq. (4.3) reduces to $1+(U_{\rm eff}/2)\Pi_{22}^0(0,0)$. This vanishes when the gap equation in Eq. (3.26) is satisfied below $T_{\rm c}$. This proves that the collective phase oscillation is always gapless at $\mathbf{q}=0$, a requirement of the Anderson-Bogoliubov (Goldstone) mode.

The b-boson Green's function consistent with treating $\hat{\Pi}$ in the HF-RPA is shown in terms of diagrams in Fig. 5(b). The result is just the same as the renormalized b-boson Green's function $\hat{D}$ given in Eq. (3.48). As discussed at the end of Sec. III B, the excitation spectrum of $\hat{D}$ is gapless at $\mathbf{q}=0$ in the superfluid phase below $T_{\rm c}$, which is again consistent with the expected gapless Bogoliubov phonon mode.

B. Goldstone mode

As discussed in the preceding section, the excitation spectrum of the renormalized b boson is determined by

$$\det[\hat{D}(\mathbf{q},i\nu_n\to\omega+i\delta)^{-1}]=0. \tag{4.6}$$

On the other hand, the collective phase oscillation and amplitude oscillation are obtained from the poles of $\hat{\Pi}$ as given by Eq. (4.2)

$$\begin{aligned}0&=\det\left[1+\frac{1}{2}[U-g_{\rm r}^2\hat{W}\hat{D}^0\hat{W}^{-1}]\hat{\Pi}^0\right]_{i\nu_n\to\omega_+=\omega+i\delta}\\&=\det[\hat{D}^0(\mathbf{q},\omega_+)]\det\left[1+\frac{U}{2}\hat{\Pi}^0(\mathbf{q},\omega_+)\right]\\&\quad\times\det\left[\hat{D}^0(\mathbf{q},\omega_+)^{-1}-\frac{g_{\rm r}^2}{4}\hat{\Xi}_U(\mathbf{q},\omega_+)\right]\\&=\frac{\det\left[1+\frac{U}{2}\hat{\Pi}^0(\mathbf{q},\omega_+)\right]}{\xi_{B\mathbf{q}}^2-\omega_+^2}\det[\hat{D}(\mathbf{q},\omega_+)^{-1}].\end{aligned} \tag{4.7}$$

Comparing Eq. (4.6) with Eq. (4.7), we see that the correlation functions Π_{ij} $(i,j=1,2)$ and the b-boson Green's function $\hat{D}$ have the identical poles (unless $\det[1+(U/2)\hat{\Pi}^0(\mathbf{q},\omega_+)]$ has zeros). This equivalence is due to hybridizing effects from the coupling between the amplitude fluctuations, phase fluctuations, and the b bosons with the amplitude-phase coupling Π_{12}^0 and the Feshbach resonance coupling $g_{\rm r}$. Thus, in principle, we can consider either one of

the correlation functions Π_{ij} or the *b*-boson Green's function $\hat{D}$ when we want to study the Goldstone mode. We choose to work with the phase correlation function Π_{22} in Eq. (4.3), in which case the dispersion relation of the collective mode is given by

$$1+\frac{V_1}{2}\tilde{\Pi}_{22}+\frac{V_2^2}{4}\frac{\Pi_{11}^0\Pi_{22}^0-\Pi_{12}^0\Pi_{21}^0}{1+\frac{V_1}{2}\Pi_{11}^0}-V_2\frac{\Pi_{12}^0}{1+\frac{V_1}{2}\Pi_{11}^0}=0. \tag{4.8}$$

Landau damping associated with thermally excited fermion quasiparticles leads to an imaginary part of the oscillation frequency and, apart from $T=0$, we have to look for a complex solution to Eq. (4.8). This requires a complicated analysis. In this paper, for simplicity, we only consider the real part of this equation [35,36],

$$\mathrm{Re}\left[1+\frac{V_1}{2}\tilde{\Pi}_{22}+\frac{V_2^2}{4}\frac{\Pi_{11}^0\Pi_{22}^0-\Pi_{12}^0\Pi_{21}^0}{1+\frac{V_1}{2}\Pi_{11}^0}-V_2\frac{\Pi_{12}^0}{1+\frac{V_1}{2}\Pi_{11}^0}\right]=0. \tag{4.9}$$

From this equation, we can obtain real frequencies as approximate solutions. In order to check the validity of this prescription, we also solve another approximate equation for the mode energy obtained from the renormalized *b*-boson Green's function,

$$\mathrm{Re}[\hat{D}_{11}^0(\mathbf{q},i\nu\rightarrow\omega_+)^{-1}]=0. \tag{4.10}$$

As for the damping of the collective mode, we investigate this effect by examining the width of the peak of the collective mode in the spectrum of the correlation functions given by $\mathrm{Im}[\Pi_{11}(\mathbf{q},\omega_+)]$ and $\mathrm{Im}[\Pi_{22}(\mathbf{q},\omega_+)]$, as well as the *b*-boson excitation spectrum given by $\mathrm{Im}[\hat{D}_{11}(\mathbf{q},i\nu_n\rightarrow\omega_+)]$. The structure function

$$S_{jj}(\mathbf{q},\omega)\equiv-\frac{1}{\pi}[n_{\mathrm{B}}(\omega)+1]\mathrm{Im}[\hat{\Pi}_{jj}(\mathbf{q},i\nu\rightarrow\omega_+)]\quad(j=1,2). \tag{4.11}$$

is more convenient than $\mathrm{Im}[\hat{\Pi}_{jj}]$ in studying collective behavior, because a diffusive mode spectrum that arises (see Sec. V D) appears as a central peak at $\omega=0$ in S_{jj}, which can be easily distinguished from collective modes appearing at a finite frequency. In contrast, this diffusive mode shows up as a peak at a *finite* frequency ω_d in $\mathrm{Im}[\hat{\Pi}_{jj}]$, which exhibits a structure of the kind $\omega/(\omega^2+\omega_d^2)$.

C. Goldstone mode at zero temperature

At zero temperature, since Landau damping is absent for modes below the excitation gap $2\tilde{\Delta}$, we can deal directly with Eq. (4.8) in determining the Goldstone mode for frequencies ω below the excitation gap. In the long wavelength or phonon limit, we take $\omega=v_\phi q$ and expand Eq. (4.8) up to the quadratic order in terms of ω and q. After some calculation, the velocity of the Goldstone mode v_ϕ is given by

$$2m\nu_\phi^2=\frac{B+\frac{1}{U_{\mathrm{eff}}^2}\frac{g_r^2}{(2\nu-2\mu)^2}}{A+\left[\eta^2\frac{U_{\mathrm{eff}}}{2}+\frac{2}{U_{\mathrm{eff}}}\frac{g_r^2}{(2\nu-2\mu)^2}\left(\frac{1+\frac{U}{2}\Pi_{11}^0(0,0)}{[2\nu-2\mu]U_{\mathrm{eff}}}-\eta\right)\right]\left[1+\frac{U_{\mathrm{eff}}}{2}\Pi_{11}^0(0,0)\right]^{-1}}. \tag{4.12}$$

The factors A and B are obtained from the expansion of Π_{22}^0 as $\Pi_{22}^0(\mathbf{q},i\nu_n)=\Pi_{22}^0(0,0)+A\nu_n^2+Bq^2/2m$, with the explicit expressions

$$A=\frac{1}{4}\sum_{\boldsymbol{p}}\frac{1}{E_{\boldsymbol{p}}^3},$$

$$B=\sum_{\boldsymbol{p}}\left[\varepsilon_{\boldsymbol{p}}\frac{\tilde{\Delta}^2}{2E_{\boldsymbol{p}}^5}+\frac{\xi_{\boldsymbol{p}}}{4E_{\boldsymbol{p}}^3}\right]. \tag{4.13}$$

Finally, the factor η is related to the amplitude-phase coupling Π_{12}^0, namely,

$$\eta\equiv\left.\frac{\Pi_{12}^0(\mathbf{q},i\nu_n)}{\nu_n}\right|_{T=\nu_n=0}=-\frac{1}{2}\sum_{\boldsymbol{p}}\frac{\xi_{\boldsymbol{p}}}{E_{\boldsymbol{p}}^3}. \tag{4.14}$$

The second term in the denominator in Eq. (4.12) describes the effect of amplitude-phase coupling (second order in η), while the second term in the numerator and the third term in the denominator involve the effect of the Feshbach resonance coupling (second order in g_{r}).

1. BCS regime: $2\nu\gg 2\varepsilon_{\mathrm{F}}$

In the BCS limit ($2\nu\gg 2\mu$), the terms involving the factor $1/(2\nu-2\mu)$ can be neglected in Eq. (4.12). In addition, since the region near the Fermi surface dominates just as in ordinary weak-coupling BCS theory, we may take

$$\sum_{\boldsymbol{p}}g(\xi_{\boldsymbol{p}})\rightarrow N(\mu(0))\int_{-\infty}^{\infty}d\xi g(\xi), \tag{4.15}$$

where $N(\mu(T=0))$ is the fermion density of states (DOS) at

the Fermi surface. In this approximation, η coming from the amplitude-phase correlation function Π_{12}^0 vanishes, and Eq. (4.12) reduces to

$$v_\phi = \frac{1}{\sqrt{2m}}\sqrt{\frac{B}{A}} = \frac{1}{\sqrt{3}}\bar{v}_{\rm F}, \tag{4.16}$$

where $\bar{v}_{\rm F} \equiv \sqrt{2\mu(0)/m}$. In evaluating B, we have approximated $\varepsilon_{\boldsymbol{p}}$ appearing in Equation (4.13) by the Fermi energy $\mu(0)$. Eq. (4.16) is the well-known velocity of the Anderson-Bogoliubov phonon in the weak-coupling BCS superfluidity [29,37,46].

The same result as in Eq. (4.16) is given by the pole of the phase correlation function Π_{22} in the BCS limit. Π_{22} in this limit is given by [taking $\Pi_{12}^0 = 0$, $V_1 = U$, and $V_2 = 0$ in Eq. (4.3)]

$$\Pi_{22}(\mathbf{q},\omega_+) = \frac{\Pi_{22}^0(\mathbf{q},\omega_+)}{1+\frac{U}{2}\Pi_{22}^0(\mathbf{q},\omega_+)} = \frac{\frac{2}{U}\Pi_{22}^0(\mathbf{q},\omega_+)}{\Pi_{22}^0(\mathbf{q},\omega_+) - \Pi_{22}^0(0,0)}. \tag{4.17}$$

Using $\Pi_{22}^0(\mathbf{q},\omega_+) = \Pi_{22}^0(0,0) - A\omega^2 + Bq^2/2m$, we easily find that the poles of Eq. (4.17) are phonons with the velocity given by Eq. (4.16). This shows that the Goldstone mode in the BCS limit is a pure collective phase oscillation of the Cooper-pair order parameter Δ.

The amplitude-phase coupling Π_{12}^0 in Eq. (3.8) vanishes in the BCS limit when we use Eq. (4.15) and retain terms up to $O(q/p_{\rm F})$, where $p_{\rm F}$=Fermi momentum. In this case, the amplitude mode is decoupled from Eq. (4.8). This mode can then be obtained from the amplitude correlation function working within the HF-RPA,

$$\Pi_{11}(\mathbf{q},\omega_+) = \frac{\Pi_{11}^0(\mathbf{q},\omega_+)}{1+\frac{U}{2}\Pi_{11}^0(\mathbf{q},\omega_+)} = \frac{\frac{2}{U}\Pi_{11}^0(\mathbf{q},\omega_+)}{\Pi_{11}^0(\mathbf{q},\omega_+) - \Pi_{22}^0(0,0)}. \tag{4.18}$$

In particular, at $\mathbf{q}=0$, Eq. (4.18) reduces to

$$\begin{aligned}\Pi_{11}(0,\omega_+) &= \frac{\Pi_{11}^0(0,\omega_+)}{UN(\mu(0))}\frac{1}{\tan^{-1}\dfrac{\omega}{\sqrt{4\Delta^2-\omega^2}}} \\ &\quad\times\frac{\omega}{\sqrt{4\Delta^2-\omega^2}} \quad (\omega\leqslant 2\Delta) \\ &\simeq \frac{2\Pi_{11}^0(0,2\Delta)}{\pi UN(\mu(0))}\frac{\Delta}{\sqrt{4\Delta^2-\omega^2}} \quad (\omega\simeq 2\Delta).\end{aligned} \tag{4.19}$$

Thus, although $\omega = 2\Delta$ is seen to be a branch cut rather than a pole, a strong peak is expected at the excitation gap $\omega = 2\Delta$ in the spectrum of the amplitude correlation function $\mathrm{Im}[\hat{\Pi}_{11}]$ and hence $S_{11}(\mathbf{q},\omega)$ [46,47].

2. BEC regime: $\nu < 0$

In the BEC regime ($\nu<0$), since the chemical potential μ approaches ν as ν decreases, the effective interaction $U_{\rm eff}$ defined in Eq. (3.2) is dominated by the Feshbach contribution $g_{\rm r}^2/(2\nu - 2\mu) \gg U$. On the other hand, the correlation functions Π_{ij}^0 become less dominant. Since $|\mu| \simeq |\nu| \gg \tilde{\Delta}$, the energy gap is also less important in the excitation spectrum of fermion quasiparticles, so that we can approximate $E_{\boldsymbol{p}} = \sqrt{(\varepsilon_{\boldsymbol{p}}-\mu)^2 + \tilde{\Delta}^2} \simeq \varepsilon_{\boldsymbol{p}} + |\nu|$. In this limiting case, Eq. (4.12) reduces to

$$v_\phi = \frac{g_{\rm r}\tilde{\Delta}}{\sqrt{8m}}\left[\sum_{\boldsymbol{p}} \frac{1}{(\varepsilon_{\boldsymbol{p}}+|\nu|)^3}\right]^{1/2} = \frac{g_{\rm r}'\tilde{\Delta}}{\sqrt{8m}}\left[\frac{3\pi}{32|\nu\varepsilon_{\rm F}|^{3/2}}\right]^{1/2}, \tag{4.20}$$

where we have rescaled the Feshbach coupling as $g_{\rm r}\sqrt{N} \to g_{\rm r}'$ in the last expression. In evaluating the $\mathbf{p}$ summation in Eq. (4.20), we have taken into account the correct energy dependence of the DOS ($\propto \sqrt{\varepsilon_{\boldsymbol{p}}}$) in contrast to the approximation in Eq. (4.15). Since $\phi_{\rm m}$ is the dominant contribution to $\tilde{\Delta}$ in the BEC regime, Eq. (4.20) is proportional to $\sqrt{N_{\rm B}^{\rm c}}$ (where $N_{\rm B}^{\rm c} = \phi_{\rm m}^2$ is the number of condensed b molecules). This dependence on $N_{\rm B}^{\rm c}$ is characteristic of the Bogoliubov phonon mode in a Bose-condensed gas. Thus, Eq. (4.20) may be regarded as the velocity of the Bogoliubov phonon associated with a condensate of b molecules. We also note that the expression in Eq. (4.20) gives as $\sim 1/|\nu|^{3/4}$ and this approaches zero when $\nu \to -\infty$. In this limit, the superfluidity is described by a BEC of a free gas with $N/2$ bosons having the particlelike excitation spectrum $\omega = q^2/2M$, with no linear (or phonon) component.

The Bogoliubov phonon associated with a Bose condensate of paired fermions has also been discussed in strong-coupling superconductivity [45], as well as for excitons in optically excited semiconductors [38]. Equation (4.12) reproduces the Bogoliubov phonon velocity in strong-coupling superconductivity [45]. In this case, the Feshbach coupling $g_{\rm r}$ and the b boson are absent, while the nonresonant interaction $-U$ is taken to be strong. Then Eq. (4.12) reduces to

$$\begin{aligned} v_\phi &= \frac{1}{\sqrt{2m}}B^{1/2}\left[A + \frac{U}{2}\frac{\eta^2}{1+\frac{U}{2}\Pi_{11}^0(0,0)}\right]^{-1/2} \\ &\to \frac{1}{\sqrt{2m}}\left[\frac{B(\tilde{\Delta}=0)}{\eta^2(\tilde{\Delta}=0)}\sum_{\boldsymbol{p}}\frac{\tilde{\Delta}^2}{(\varepsilon_{\boldsymbol{p}}+|\mu|)^3}\right]^{1/2} = \frac{\tilde{\Delta}}{\sqrt{8m|\mu|}},\end{aligned} \tag{4.21}$$

where we have taken the strong-coupling limit ($U\to\infty$), with μ large and negative. The last expression can be shown to be equivalent to the Bogoliubov phonon velocity in strong coupling superconductivity, as discussed in Ref. [45]. Using the strong-coupling expressions, $\tilde{\Delta} = (16/3\pi)^{1/2}\varepsilon_{\rm F}/\sqrt{p_{\rm F}a_s}$

and $\mu=-1/2ma_s^2$ [45], where a_s is an *s*-wave scattering length of the pairing interaction between fermions and p_F is the Fermi momentum, Eq. (4.21) reduces to a more familiar form

$$v_\phi=\left[\frac{n_B U_B}{M}\right]^{1/2}. \tag{4.22}$$

Here, $n_B\equiv N/2V$ is the number density of Cooper-pair bosons (where V is the volume of a system) and $U_B \equiv 4\pi a_B/M$ $(M=2m)$ is an effective interaction between Cooper pairs with an *s*-wave scattering length $a_B\equiv 2a_s$. Here $U_{\rm eff}=-4\pi a_s/m$ is defined as in Eq. (3.2).

V. BCS-BEC CROSSOVER IN THE SUPERFLUID PHASE: NUMERICAL RESULTS

In this section, we present numerical results for the various thermodynamic parameters and correlation functions discussed in earlier sections, as one passes through the BCS-BEC crossover region. We give results as a function of the temperature in the superfluid phase ($T<T_c$) for different values of the *b*-molecule threshold 2ν. We take the Fermi energy ε_F, Fermi momentum p_F, and Fermi velocity v_F as the units of energy, momentum and velocity, respectively, where ε_F, p_F, and v_F are all in the absence of coupling to *b* bosons. As the unit for the number for particles, we take the total number of Fermi atoms *N*. Since the interactions *U* and g_r always appear with *N* as UN and g_r^2N, we rescale them as $UN\to U$ and $g_r\sqrt{N}\to g_r$. As for the energy cutoff that is necessary in the gap equation in Eq. (3.16) and the correlation functions Π_{ij}^0 in Eqs. (3.20)–(3.25), we employ the Gaussian cutoff $e^{-(\varepsilon_p/\omega_c)^2}$ with $\omega_c=2\varepsilon_F$, as in our previous work for T_c [12–14]. This choice of cutoff seems reasonable. Different cutoff magnitudes are physically equivalent to changing the magnitude of the effective pairing interaction. These different cutoffs $\omega_c\sim\varepsilon_F$ will lead to quantitative changes in the size of the BCS-BEC crossover. We refer to Refs. [14,11] for further discussion of the choice of cutoff and renormalized interactions.

Since our ''strong-coupling'' theory is based on perturbative expansions with respect to $-U$ and g_r, these coupling terms are assumed to be weak perturbations. For this reason, we take $g_r=0.6\varepsilon_F$ and $U=0.3\varepsilon_F$ in all our numerical calculations. In Sec. IV of Ref. [14], we have discussed the transition temperature T_c in the BCS-BEC crossover for the case of a very broad [11,15] Feshbach resonance ($g_r\gg\varepsilon_F$). In this case, the Cooper pairs dominate in the crossover region, which occurs at large values of ν. Analogous results would be expected in the superfluid region discussed in the present paper.

A. Temperature dependence of the order parameter and chemical potential

The self-consistent solutions $(\tilde\Delta,\mu)$ of the coupled equations (3.16) and (3.41) are shown in Figs. 6 and 7. In Fig. 6(a), we find that the temperature dependence of the order parameter $\tilde\Delta\equiv\Delta-g_r\phi_m$ agrees well with the BCS theory (''BCS'' in the figure). Since $\tilde\Delta$ determines the energy gap of the fermion quasiparticle spectrum as $E_p=\sqrt{\xi_p^2+\tilde\Delta^2}$, the superfluid character at $\nu/\varepsilon_F=2$ is found to be the BCS type. However, Fig. 6(a) also shows a sizable difference between $\tilde\Delta$ and the Cooper-pair amplitude $\Delta=\Sigma_p\langle c_{-p\downarrow}c_{p\uparrow}\rangle$. This is because the BEC order parameter $\phi_m=\langle b_{q=0}\rangle$ is always induced below T_c due to the Feshbach coupling effect in Eq. (2.5), which contributes to $\tilde\Delta=\Delta-g_r\phi_m$. As illustration, when we substitute $\nu/\varepsilon_F=2$, $g_r/\varepsilon_F=0.6$, $U/\varepsilon_F=0.3$, and $\mu/\varepsilon_F\simeq 0.84$ into Eq. (2.5), the contribution of the condensed *b* boson to $\tilde\Delta$ is found to be $-g_r\phi_m=0.517\Delta$ at $T=0$. This

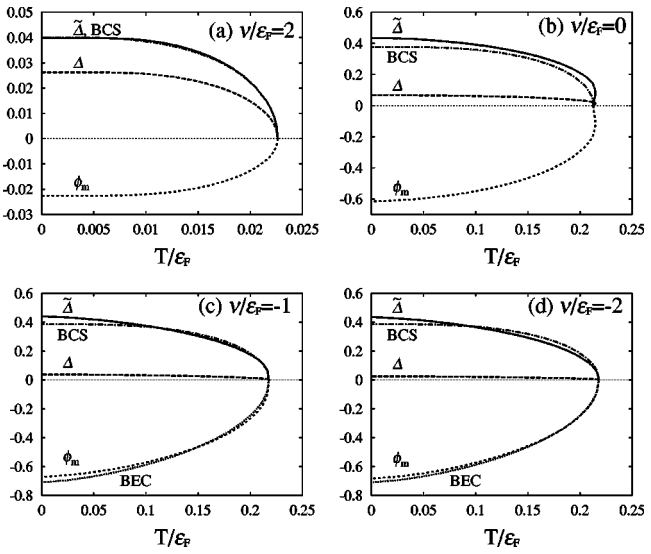

FIG. 6. Temperature dependence of the superfluid order parameter $\tilde\Delta\equiv\Delta-g_r\phi_m$ in the BCS-BEC crossover region. We also show the separate Cooper-pair component Δ and the Bose-condensed *b*-molecule component ϕ_m. We take $g_r/\varepsilon_F=0.6$ and $U/\varepsilon_F=0.3$, while $\tilde\Delta$ and Δ are normalized with respect to ε_F. The character of the superfluidity changes from the BCS type to the BEC type as one goes from (a) to (d). In this figure, BCS labels the order parameter given by the weak-coupling BCS theory which omits the particle-particle fluctuations. BEC labels the order parameter ϕ_m of a free Bose gas of $N/2$ atoms. Note the change in scale in (a).

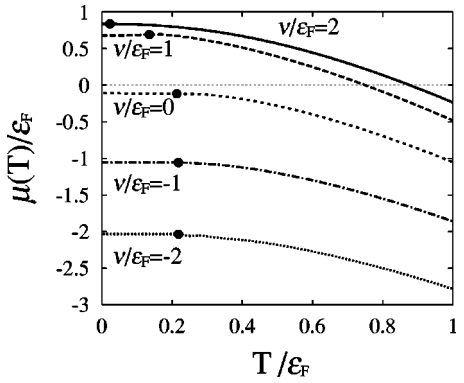

FIG. 7. The chemical potential μ as a function of temperature, for $g_r/\varepsilon_F=0.6$ and $U/\varepsilon_F=0.3$. The solid circles show the superfluid phase transition temperature.

means about one-third of the order parameter $\tilde{\Delta}$ is associated with $\phi_{\rm m}$ even in the BCS regime at $\nu/\varepsilon_{\rm F}=2$.

As the threshold energy 2ν is lowered, the Cooper-pair component Δ becomes less dominant while the condensed b boson component $\phi_{\rm m}$ increases [Fig. 6(a) $\rightarrow$ 6(d)]. At the same time, the temperature dependence of $\tilde{\Delta}$ deviates from the weak-coupling BCS theory. At $\nu/\varepsilon_{\rm F}=-2$ in Fig. 6(d), $\tilde{\Delta}$ is dominated by $\phi_{\rm m}$ (although the Cooper-pair component also exists due to the Feshbach coupling effect). In this case, $\phi_{\rm m}$ is well described by the BEC order parameter of $N/2$ atoms in a free Bose gas, given by

$$\phi_{\rm m}^{\rm BEC}=\sqrt{\frac{N}{2}}\sqrt{1-\left(\frac{T}{T_{\rm c}}\right)^{3/2}}. \tag{5.1}$$

We denote $\phi_{\rm m}^{\rm BEC}$ in Fig. 6 as "BEC."

In the intermediate region of the BCS-BEC crossover, $\tilde{\Delta}$ (and also Δ and $\phi_{\rm m}$) becomes double valued near $T_{\rm c}$. For example, in Fig. 6(b), the two self-consistent values for $\tilde{\Delta}$ at $T_{\rm c}=0.213T_{\rm F}$ ($\equiv T_{\rm c}^{\rm L}$, where L stands for lower transition temperature) are zero and $0.14\varepsilon_{\rm F}$. In this case, when one decreases the temperature, $\tilde{\Delta}$ jumps abruptly at $T_{\rm c}^{\rm L}$. This is because the phase transition is suppressed by superfluid particle-particle fluctuations, once the phase transition occurs, the opening up of the fermion quasiparticle excitation gap $2\tilde{\Delta}$ strongly suppresses these fluctuation effects, which accelerates the increase of $\tilde{\Delta}$. On the other hand, when we raise the temperature from below, since the superfluid fluctuations are suppressed by the excitation gap, we can exceed $T_{\rm c}^{\rm L}$ staying in the superfluid phase up to a higher temperature ($\equiv T_{\rm c}^{\rm H}$). In Fig. 6(b), we see that $T_{\rm c}^{\rm H}=0.215T_{\rm F}$, slightly higher than $T_{\rm c}^{\rm L}$. At $T_{\rm c}^{\rm H}$, $\tilde{\Delta}$ vanishes discontinuously. This kind of the first-order transition has been discussed in the literature of high-$T_{\rm c}$ superconductivity with strong fluctuations in the Cooper channel [48]

Figure 7 shows that the chemical potential μ is decreased as the system approaches the BEC regime ($\nu<0$). The temperature dependence of μ is found to be weak below $T_{\rm c}$ (except just below $T_{\rm c}$ in the crossover regime) compared with the normal phase. As discussed in Sec. III, the chemical potential is temperature independent below $T_{\rm c}$ in both the BCS limit ($\mu=\varepsilon_{\rm F}$) and the BEC limit ($\mu=\nu$). Figure 7 shows that this feature also holds in the intermediate region of the BCS-BEC crossover except just below $T_{\rm c}$, at least for the model parameters we have chosen.

Now that we have calculated self-consistently the values of the composite order parameter $\tilde{\Delta}$ as function of both T and 2ν, we can use the results to discuss the spectrum of the BCS-Bogoliubov single-particle Green's function. The excitation spectrum of the BCS-Bogoliubov quasiparticles is given by

$$\rho_{\rm F}(\omega)\equiv-\frac{1}{\pi}\sum_{\boldsymbol{p}}\ {\rm Im}[\hat{G}_{11}(\mathbf{p},i\omega_m\rightarrow\omega+i\delta)], \tag{5.2}$$

where $\hat{G}_{11}(\mathbf{p},\omega+i\delta)$ is the (11)-component of Eq. (3.11). When the chemical potential μ is positive, the excitation spectrum in Eq. (5.2) has a finite gap $\tilde{\Delta}$ as in the BCS theory,

$$\begin{aligned}\rho_{\rm F}(\omega,\mu\geqslant 0)=\frac{3N}{8\varepsilon_{\rm F}^{3/2}}\Bigg[&\left(\frac{\omega}{\sqrt{\omega^2-\tilde{\Delta}^2}}+1\right)(\mu+\sqrt{\omega^2-\tilde{\Delta}^2})^{1/2}\\&+\left(\frac{\omega}{\sqrt{\omega^2-\tilde{\Delta}^2}}-1\right)(\mu-\sqrt{\omega^2-\tilde{\Delta}^2})^{1/2}\\&\times\Theta(\sqrt{\tilde{\Delta}^2+\mu^2}-\omega)\Bigg]\Theta(\omega-\tilde{\Delta}),\end{aligned} \tag{5.3}$$

where $\Theta(x)$ is the step function. On the other hand, when μ is negative in the BEC regime, one finds

$$\begin{aligned}\rho_{\rm F}(\omega,\mu<0)=&\frac{3N}{8\varepsilon_{\rm F}^{3/2}}\left(\frac{\omega}{\sqrt{\omega^2-\tilde{\Delta}^2}}+1\right)\\&\times(\mu+\sqrt{\omega^2+\tilde{\Delta}^2})^{1/2}\Theta(\omega-\sqrt{\tilde{\Delta}^2+\mu^2}).\end{aligned} \tag{5.4}$$

In this case, the Fermi quasiparticle excitation gap is found to be $\sqrt{\tilde{\Delta}^2+\mu^2}$, rather than $\tilde{\Delta}$. This reflects the fact that the threshold energy of free fermion excitations is given by $|\mu|$ when $\mu<0$. In the BEC limit ($\mu\simeq\nu\ll-\varepsilon_{\rm F}$), we have $|\mu|\gg\tilde{\Delta}$ and the excitation gap reduces to $|\mu|$.

Figure 8(a) shows the excitation spectrum of the BCS-Bogoliubov quasiparticles in the BCS-BEC crossover. In the BCS regime ($\nu\geqslant\varepsilon_{\rm F}$), we find a peak at the excitation edge $\omega=\tilde{\Delta}$ in the spectrum. This is the well-known coherence peak discussed in the superconductivity literature [37], and the quasiparticle spectrum is found to be the BCS type in this regime. This coherence is absent when $\nu\leqslant 0$, where the excitation gap gradually changes from $\tilde{\Delta}$ to $|\mu|$ as the threshold energy 2ν is lowered. Since $\mu\simeq\nu$ in the BEC regime, the energy gap ($\sqrt{\mu^2+\tilde{\Delta}^2}$) becomes larger for lower values of ν in the BEC regime.

Figure 8(b) shows the momentum distribution function of Fermi atoms at $T=0$ [37], which is given by

$$v_{\mathbf{p}}^2\equiv\langle c_{\boldsymbol{p}\sigma}^{\dagger}c_{\boldsymbol{p}\sigma}\rangle=\frac{1}{2}\left(1-\frac{\xi_{\boldsymbol{p}}}{E_{\boldsymbol{p}}}\right). \tag{5.5}$$

Since the energy gap $\tilde{\Delta}$ in $E_{\boldsymbol{p}}=\sqrt{\xi_{\boldsymbol{p}}^2+\tilde{\Delta}^2}$ is larger for smaller values of the threshold energy 2ν, the steep decrease of $v_{\boldsymbol{p}}^2$ around $\mu(T=0)$ at $\nu/\varepsilon_{\rm F}=2$ gradually disappears as 2ν is lowered. In addition, the magnitude of $v_{\boldsymbol{p}}^2$ decreases as one approaches the BEC regime due to the decrease of the chemical potential $\mu(T=0)$, which reflects the fact that most Fermi atoms form b bosons in the BEC regime. The quantity $v_{\boldsymbol{p}}$ also enters into the Bogoliubov transformation [37] to the BCS quasiparticles

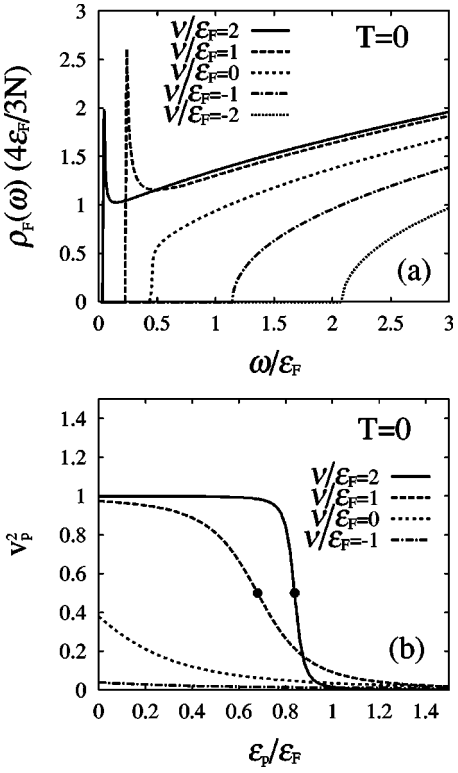

FIG. 8. (a) Density of states of the BCS-Bogoliubov quasiparticles at $T=0$. For $\nu/\varepsilon_F \geqslant 1$, the threshold energy of the quasiparticle excitations is given by $\omega=\tilde{\Delta}$, at which a coherence peak appears. For $\nu/\varepsilon_F \leqslant 0$, the coherence peak is absent and the spectrum starts from $\omega=(\mu^2+\tilde{\Delta}^2)^{1/2}$. The excitation density of states approaches that for a free Fermi gas of atoms $\rho_F(\omega)=(3N/4\varepsilon_F^{3/2})(\omega+\mu)^{1/2}$ in the high-energy region. (b) Momentum distribution function $v_p^2 \equiv \langle c_{p\sigma}^\dagger c_{p\sigma}\rangle$ of Fermi atoms with σ-spin component at $T=0$. The solid circle indicates the chemical potential $\mu(T=0)$.

$$\gamma_{p\uparrow}^\dagger = u_p c_{p\uparrow}^\dagger + v_p c_{-p\downarrow}, \tag{5.6}$$

where $\gamma_{p\uparrow}^\dagger$ is a creation operator of a BCS-Bogoliubov quasiparticle and $u_p^2 \equiv 1-v_p^2$.

B. Velocity of the Goldstone phonon mode

Figure 9 shows the velocity of the Goldstone mode v_ϕ at

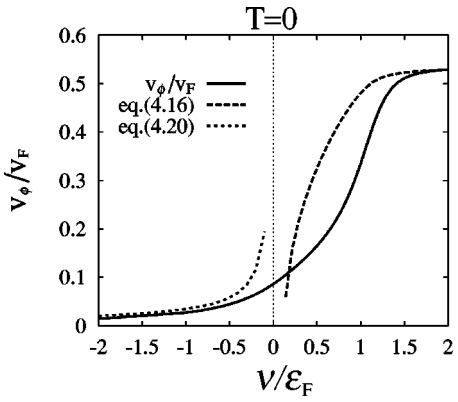

FIG. 9. Velocity of the Goldstone phonon v_ϕ (normalized to the Fermi velocity) at $T=0$ in the BCS-BEC crossover region.

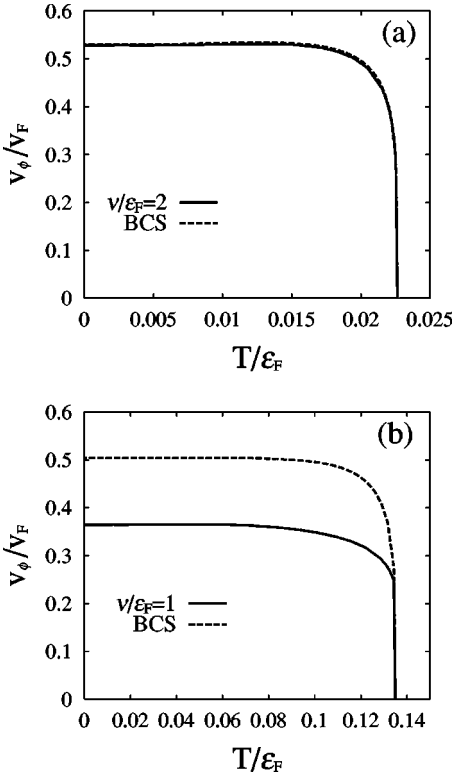

FIG. 10. Temperature dependence of the Goldstone phonon velocity v_ϕ, (a) $\nu/\varepsilon_F=2$, (b) $\nu/\varepsilon_F=1$. BCS labels the Anderson-Bogoliubov phonon velocity given by the weak-coupling BCS theory, where we use T_c from Fig. 2 and μ from Fig. 7.

$T=0$ as obtained from Eq. (4.12). In the BCS regime ($\nu \gtrsim \varepsilon_F$), the mode velocity v_ϕ agrees with the well-known Anderson-Bogoliubov phonon velocity $v_\phi=\overline{v_F}/\sqrt{3}$ in Eq. (4.16). [At $\nu/\varepsilon_F=2$, we obtain $\overline{v_F}=\sqrt{2\mu(0)/m}=0.92v_F$ for $\mu(0)\simeq 0.84\varepsilon_F$, which gives $v_\phi=0.53v_F$.] As the threshold energy 2ν is lowered, v_ϕ decreases sharply and approaches the Bogoliubov phonon mode given by Eq. (4.20). Figure 9 indicates that v_ϕ is strongly dependent on the threshold energy 2ν in a uniform Fermi gas.

Figure 10 shows the velocity of the Goldstone mode at finite temperatures, obtained from Eq. (4.9). In Fig. 10(a), v_ϕ is found to be well described by the Anderson-Bogoliubov mode in the weak-coupling BCS theory (BCS in the figure) in the whole temperature region, as expected for the value $\nu=2\varepsilon_F$. On the other hand, v_ϕ becomes less than the BCS result for the Anderson-Bogoliubov mode as the threshold energy 2ν is decreased. This is shown in Fig. 10(b). Since the order parameter $\tilde{\Delta}$ vanishes discontinuously due to the fluctuation effect discussed in the preceding section, v_ϕ shows a finite jump at T_c in Fig. 10(b).

C. Dispersion relation of the Goldstone mode

Figure 11 shows the dispersion of the Goldstone mode at $T=0.5T_c$. In the BCS regime [Fig. 11(a)], the gapless dispersion is convex and is confined below the excitation gap at $2\tilde{\Delta}$. This convex dispersion relation gradually changes to a concave one as one goes from panels (a) to (d) in Fig. 11. In

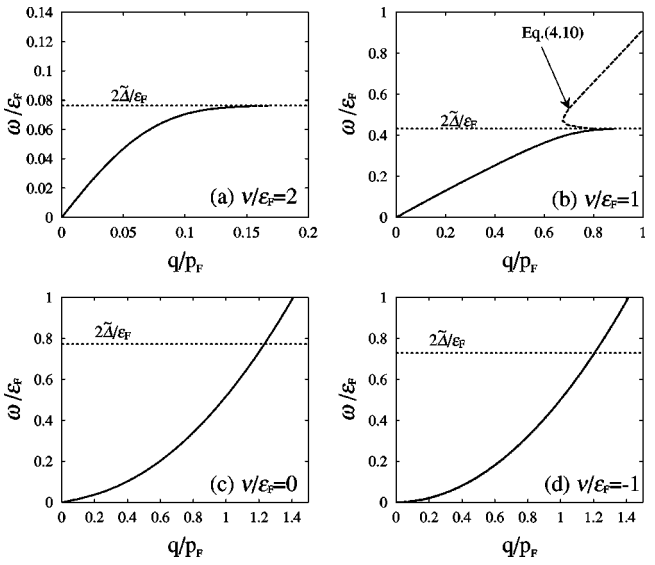

FIG. 11. Dispersion relation of the Goldstone mode at $T=0.5T_c$ for different values of ν. The solid lines show the dispersion obtained from Eqs. (4.9) and (4.10). At $\nu/\varepsilon_F=2$, Eq. (4.10) has an additional very high-energy solution around $\omega/\varepsilon_F=2.4$ (see Fig. 12).

the BEC limit ($\nu<0$), the dispersion is particlelike q^2, characteristic of free b bosons. Indeed, the dispersion in Fig. 11(d) is well described by $\omega=q^2/2M$, except for the region of linear dispersion $\omega=v_\phi q$ at very small q.

In the BCS regime, Eq. (4.10) also has a high-energy solution at $\omega/\varepsilon_F\simeq 2.4$, as shown in Fig. 12. This solution is also obtained at T_c. Since the energy of this solution is close to the threshold energy of the excitation spectrum of free b bosons as $\xi_{B\boldsymbol{q}=0}=2\nu-2\mu=2.32\varepsilon_F$ ($\mu\simeq 0.84\varepsilon_F$), we interpret this high-energy solution as an internal excitation of a b boson. They are not the amplitude oscillations of the order parameter.

Finally, we briefly comment on the approximate Eqs. (4.9) and (4.10). Since the excitation gap $2\tilde{\Delta}$ strongly suppresses the fermion quasiparticle excitations far below T_c,

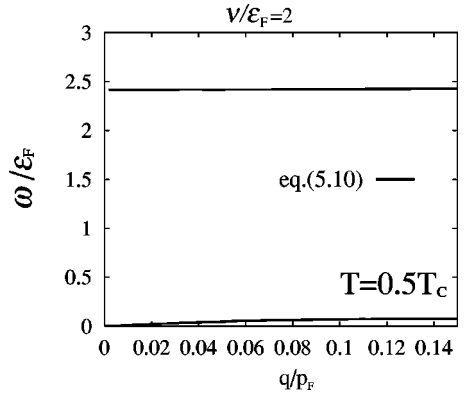

FIG. 12. The high-energy solution of Eq. (4.10) in the case of $\nu/\varepsilon_F=2$, for $T=0.5T_c$. The lower-energy solution is the Goldstone mode, shown in Fig. 11(a).

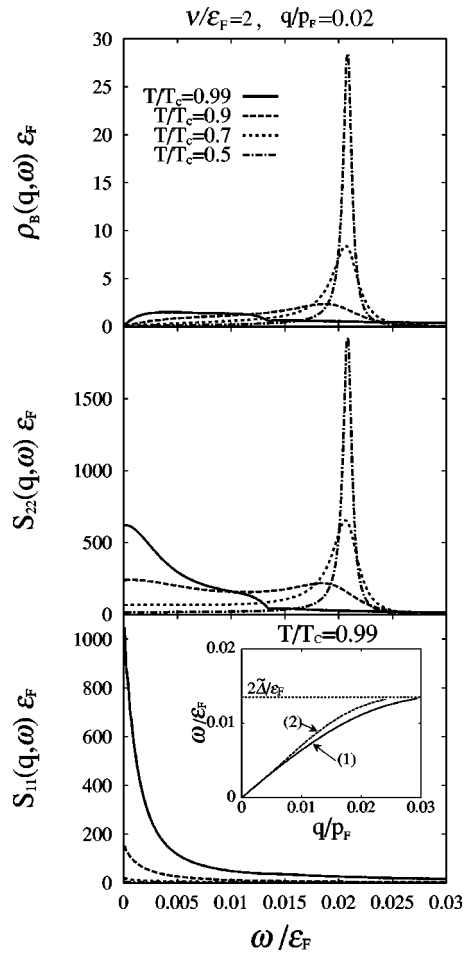

FIG. 13. Spectral weight of the renormalized b boson, $\rho_B(\mathbf{q},\omega)=-(1/\pi)\mathrm{Im}[\hat{D}_{11}(\mathbf{q},\omega)]$, and the structure functions $S_{11}(\mathbf{q},\omega)$ and $S_{22}(\mathbf{q},\omega)$. These results are for $\nu=2\varepsilon_F$ (in the BCS region) and $q=0.02p_F$. The inset shows two different approximations for the dispersion relation of the Goldstone mode at $T/T_c=0.99$: (1) and (2) are obtained from Eqs. (4.9) and (4.10), respectively.

the intraband terms of Π^0_{ij} and also the Landau damping below $2\tilde{\Delta}$ are less important at $T=0.5T_c$. As a result, Eqs. (4.9) and (4.10) both give good approximations to the solution of Eq. (4.7) at $T=0.5T_c$, and give almost the same results below $2\tilde{\Delta}$, as shown in Figs. 11(a) and 11(b) (solid lines). On the other hand, the interband terms given by the second lines in Eqs. (3.20)–(3.25) give rise to Landau damping when $\omega\geqslant 2\tilde{\Delta}$. Thus, above $2\tilde{\Delta}$, Eqs. (4.9) and (4.10) may have different solutions, because they do not include the imaginary part in the same way. Indeed, the dashed line above $2\tilde{\Delta}$ shown in Fig. 11(b) is a solution of Eq. (4.10), but is not obtained from Eq. (4.9). In such a case, a more careful analysis is necessary to obtain the correct dispersion relation. However, since the fermion quasiparticles are absent in the BEC limit ($\nu<0$), the Landau damping becomes weak in the BEC regime even near T_c. As a result, Eqs. (4.9) and

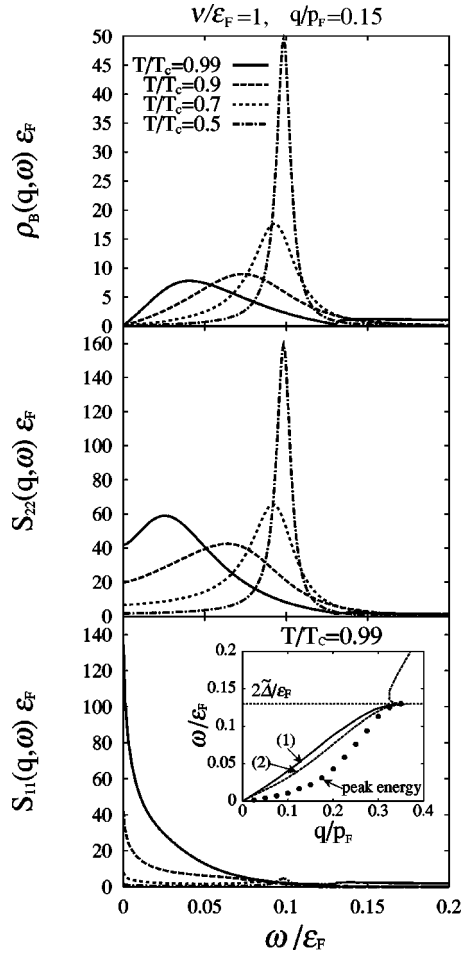

FIG. 14. Same plots as in Fig. 13, for $\nu=\varepsilon_{\mathrm{F}}$ and $q=0.15p_{\mathrm{F}}$. In the inset, the peak energy gives the peak position in $S_{22}(\mathbf{q},\omega)$ at $T/T_{\mathrm{c}}=0.99$.

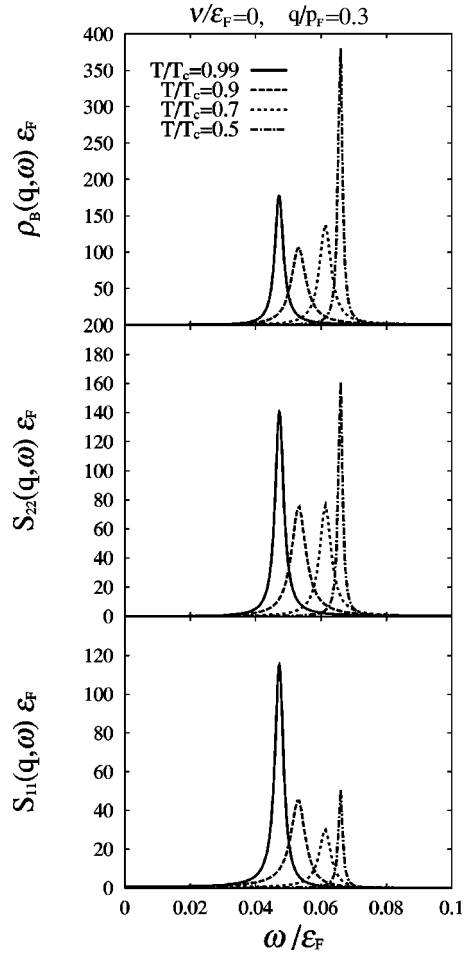

FIG. 15. Same plots as in Fig. 13, for $\nu=0$ (crossover region) and $q=0.3p_{\mathrm{F}}$.

(4.10) give almost identical results in the whole energy region.

D. Spectral weight and damping of the Goldstone mode

In Secs. V B and V C, we considered the Goldstone mode neglecting the Landau damping. In this section, we evaluate the damping from the width of the collective mode in the structure function $S_{jj}(\mathbf{q},\omega_+)$ in Eq. (4.11) as well as in the *b*-boson spectral density

$$\rho_{\mathrm{B}}(\mathbf{q},\omega)\equiv-\frac{1}{\pi}\mathrm{Im}[\hat{D}_{11}(\mathbf{q},\omega_+)]. \tag{5.7}$$

In Figs. 13–16, we show the *b*-boson excitation spectrum, as well as the phase S_{22} and amplitude S_{11} structure functions for T, below T_{c}. In Fig. 13, we find that the Anderson-Bogoliubov Goldstone mode does not appear as a visible peak in the spectrum at $T/T_{\mathrm{c}}=0.99$. (The inset in Fig. 13 shows that the mode energy is $\omega/\varepsilon_{\mathrm{F}}=0.01$ for $q=0.02p_{\mathrm{F}}$.) This means that the Anderson-Bogoliubov mode is overdamped near T_{c} because of strong Landau damping from the thermally excited fermion quasiparticles. We note that $S_{22}(\mathbf{q},\omega)$ and $S_{11}(\mathbf{q},\omega)$ both exhibit strong central peaks at $\omega=0$ for $T/T_{\mathrm{c}}=0.99$, which indicates the presence of a large number of thermally excited fermion quasiparticles expected at this temperature. This collective mode in the thermally excited fermions has been discussed in superconductivity literature [35].

At low temperatures, when the Landau damping becomes weaker, the Anderson-Bogoliubov mode appears as a visible peak in $\rho_{\mathrm{B}}(\mathbf{q},\omega)$ and $S_{22}(\mathbf{q},\omega)$ as shown in Fig. 14. The peak width becomes narrower at lower temperatures, reflecting the weaker Landau damping by fermions. (At $T=0$, it becomes a sharp δ-function peak.) The peak position ($\omega/\varepsilon_{\mathrm{F}}\simeq0.021$) at $T/T_{\mathrm{c}}=0.5$ agrees well with the dispersion relation shown in Fig. 11(a).

Since the Anderson-Bogoliubov mode is a collective phase oscillation of the Cooper-pair order parameter Δ, the appearance of this mode in $\rho_{\mathrm{B}}(\mathbf{q},\omega)$ indicates the presence of the coupling between the *b* bosons and the phase fluctuations of Δ. On the other hand, no peak structure is observed except for the central peak at $\omega=0$ in the amplitude structure function S_{11} shown in Fig. 13. Only a slight structure appears at $\omega/\varepsilon_{\mathrm{F}}\simeq0.02$ at $T/T_{\mathrm{c}}=0.7$, as shown in part (a) of Fig. 17. (The peak at $\omega/\varepsilon_{\mathrm{F}}\simeq0.07$ in Fig. 17 is the amplitude mode at the edge of interband excitations $\omega=2\tilde{\Delta}$.) This is because the amplitude-phase coupling Π_{12}^{0} is very weak in the BCS

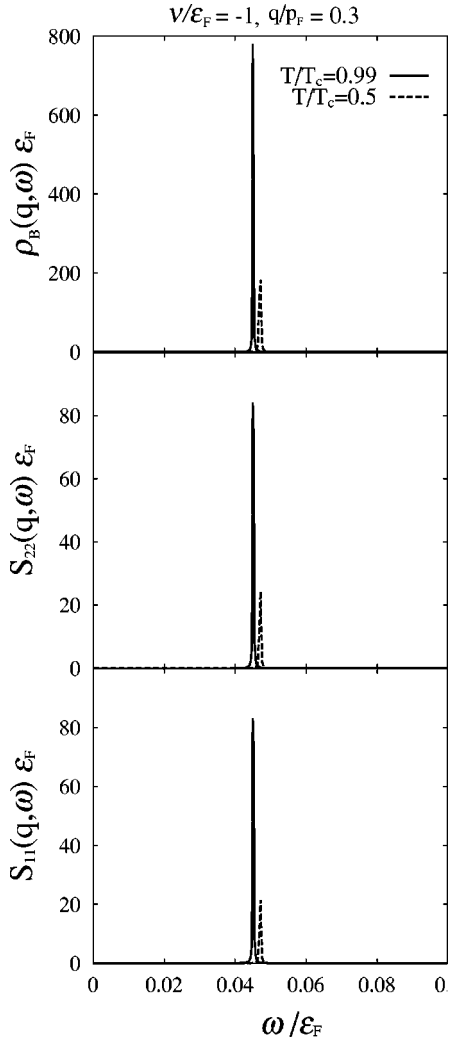

FIG. 16. Same plots as in Fig. 13 for $\nu=-\varepsilon_{\mathrm{F}}$ (BEC region) and $q=0.3p_{\mathrm{F}}$.

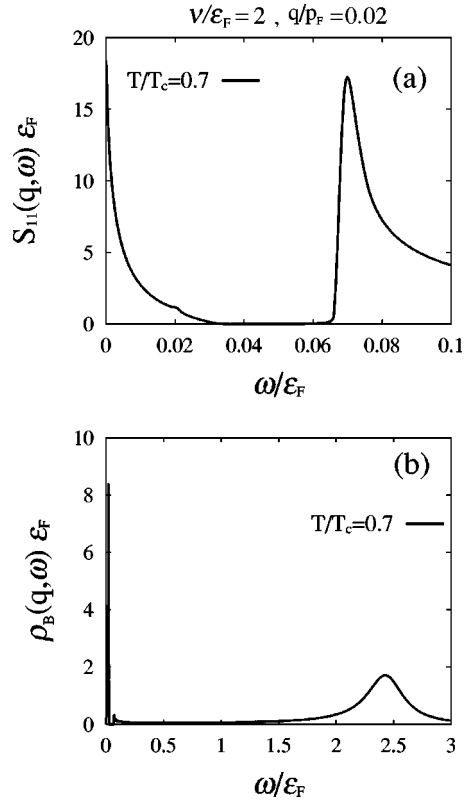

FIG. 17. The amplitude structure function $S_{11}(\mathbf{q},\omega)$ is shown in (a) and the b-boson spectrum $\rho_{\mathrm{B}}(\mathbf{q},\omega)$ is shown in (b) for $\nu/\varepsilon_{\mathrm{F}}=2$ (BCS region) and $T/T_{\mathrm{c}}=0.7$. In panel (a) the extremely small structure visible at $\omega/\varepsilon_{\mathrm{F}}\simeq 0.02$ is due to the Anderson-Bogoliubov mode. The larger peak at $\omega/\varepsilon_{\mathrm{F}}\simeq 0.07$ is the amplitude mode. However, since the excitation gap is also at $2\tilde{\Delta}=0.068$, this mode coincides with the edge of the interband excitations. In panel (b) the peak on the left is the Anderson-Bogoliubov mode, while the broad peak at $\omega/\varepsilon_{\mathrm{F}}$ corresponds to the high-energy solution shown in Fig. 12. A very small peak at $\omega/\varepsilon_{\mathrm{F}}\simeq 0.068$ in panel (b) is located at the excitation gap $2\tilde{\Delta}$.

regime, so that the collective phase oscillation does not strongly couple into the amplitude fluctuations.

As shown in Fig. 12, Eq. (4.10) also has a high-energy solution in the BCS regime at $\nu/\varepsilon_{\mathrm{F}}=2$. This solution is the strong resonance in $\rho_{\mathrm{B}}(\mathbf{q},\omega)$, as shown in part (b) of Fig. 17.

In Fig. 14, we find a broad peak in S_{22} at $T/T_{\mathrm{c}}=0.99$. As shown in the inset in Fig. 14, the peak position is different from the one expected from Eqs. (4.9) and (4.10). However, since this resonance shows gapless behavior, it clearly must be the Goldstone mode. (The difference shown in the inset is due to the Landau-damping effect.) Indeed, the peak energy at $T/T_{\mathrm{c}}=0.5$ agrees well with the dispersion in Fig. 11(b). As expected, Landau damping from fermions becomes weak as one approaches the BEC regime. When $\nu\leqslant 0$, we can observe the sharp peak structure even near T_{c} in Figs. 15 and 16, and the peak position always agrees well with the dispersion relation given in Fig. 11. The dispersion relation of the Goldstone mode approaches the temperature-independent particlelike one in the BEC regime, and hence the temperature dependence of the peak energy in Fig. 16 is weak.

We also find in Figs. 14–16 that the Goldstone mode appears in the amplitude structure factor $S_{11}(\mathbf{q},\omega)$, which indicates that the amplitude-phase coupling becomes stronger as 2ν is decreased. Although the amplitude fluctuations described by Π_{11} are not important in the BCS regime, we cannot neglect these fluctuations in the BCS-BEC crossover regime.

VI. DENSITY-DENSITY CORRELATION FUNCTION

An important problem is how to experimentally observe the Goldstone mode discussed in Secs. IV and V. In this section, we show that the density-density correlation function Π_{33} defined in Eq. (3.19) exhibits this mode as a pole. This correlation function can be experimentally probed by many techniques, including two-photon Bragg scattering [49].

Since the Goldstone mode is associated with the collective phase fluctuations of the Cooper pairs, a coupling between density fluctuations and phase fluctuations is necessary in order for the Goldstone mode to appear in the spectrum exhibited by $\Pi_{33}(\mathbf{q},\omega_{+})$. In this regard, we note

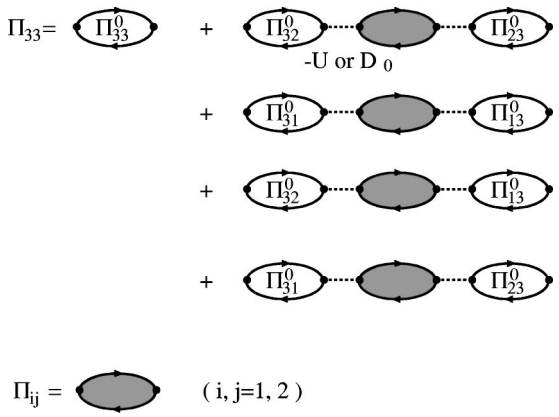

FIG. 18. The density-density correlation function Π_{33} coupled with superfluid amplitude and phase fluctuations described by Π_{ij} $(i,j=1,2)$ (shaded bubbles). Π^0_{23} and Π^0_{32} describe phase-density correlations, while Π^0_{13} and Π^0_{31} give the amplitude-density correlations.

that a phase-density coupling exists in fermion superfluidity because of the presence of the Josephson effect. This coupling is described by Π^0_{23} (and Π^0_{32}) defined in Eq. (3.24). In contrast to the amplitude-phase correlation function Π^0_{12}, which is very weak in the BCS regime, Π^0_{23} is finite even if one works with the approximation in Eq. (4.15). Besides Π^0_{23}, density fluctuations also couple with superfluid fluctuations through amplitude-density coupling Π^0_{13} (and Π^0_{31}) defined in Eq. (3.25). This coupling is not important in the BCS regime, because Π^0_{13} vanishes when one uses the approximation in Eq. (4.15) and neglects terms of the order of $O((q/p_F)^2)$). However, as in the case of the amplitude-phase correlation function Π^0_{12}, this coupling effect becomes stronger as one goes into the BCS-BEC crossover regime. Then the density-density correlation function Π_{33} is found to couple with superfluid fluctuations (amplitude and phase) via Π^0_{23} and Π^0_{13}, as shown diagrammatically in Fig. 18.

The density-density correlation function Π_{33} given by the HF-RPA is obtained by extending the method discussed in Sec. IV of Ref. [40]. When we introduce a 3×3-matrix correlation function $\hat{\Pi}=\{\Pi_{ij}\}$ $(i,j=1,2,3)$, which involves the density-density correlation function as the (33)-component, we obtain an equation similar to Eq. (4.2), namely,

$$\hat{\Pi}=\hat{\Pi}^0\left[1+\frac{1}{2}\bar{U}\hat{\Pi}^0\right]^{-1}. \tag{6.1}$$

Here, the interaction 3×3 matrix $\bar{U}$ is defined by

$$\bar{U}\equiv\begin{pmatrix}\bar{U}_{11} & \bar{U}_{12} & 0\\ \bar{U}_{21} & \bar{U}_{22} & 0\\ 0 & 0 & 0\end{pmatrix}, \tag{6.2}$$

where $\bar{U}_{ij}\equiv\{U-g_r^2\hat{W}\hat{D}^0\hat{W}^{-1}\}_{ij}$. If we include a density-density interaction term to our coupled fermion-boson model in Eq. (2.1), it would be included as the (3,3)-component in Eq. (6.2). The density-density correlation function is obtained from the (3,3)-component of Eq. (6.1),

$$\Pi_{33}=\Pi^0_{33}+\frac{\bar{\Pi}_{33}}{1+\frac{V_1}{2}[\Pi^0_{11}+\Pi^0_{22}]-\frac{V_1}{2}[\Pi^0_{12}-\Pi^0_{21}]+\left[\frac{V_1^2}{4}+\frac{V_2^2}{4}\right][\Pi^0_{11}\Pi^0_{22}-\Pi^0_{12}\Pi^0_{21}]}, \tag{6.3}$$

where the numerator is

$$\begin{aligned}\bar{\Pi}_{33}\equiv&\left[\frac{V_1^2}{4}+\frac{V_2^2}{4}\right][\Pi^0_{31}\Pi^0_{12}\Pi^0_{23}-\Pi^0_{31}\Pi^0_{22}\Pi^0_{13}+\Pi^0_{32}\Pi^0_{21}\Pi^0_{13}\\&-\Pi^0_{32}\Pi^0_{11}\Pi^0_{23}]-\frac{V_1}{2}[\Pi^0_{31}\Pi^0_{13}+\Pi^0_{32}\Pi^0_{23}]\\&-\frac{V_2}{2}[\Pi^0_{31}\Pi^0_{23}-\Pi^0_{32}\Pi^0_{13}].\end{aligned} \tag{6.4}$$

Each term in Eq. (6.4) involves correlation functions between density fluctuations and superfluid fluctuations, such as Π^0_{23} and Π^0_{13}.

Figure 19 shows the dynamic structure function related to the spectral density of the density-density correlation function

$$S_{33}(\mathbf{q},\omega)\equiv-\frac{1}{\pi}[n_B(\omega)+1]\mathrm{Im}[\Pi_{33}(\mathbf{q},i\nu_n\to\omega_+)]. \tag{6.5}$$

At low temperatures in Figs. 19(a) and 19(b) (BCS regime), and at all the temperatures in Figs. 19(c) and 19(d) (BEC regime), we can clearly see the Goldstone mode as a resonant peak in $S_{33}(\mathbf{q},\omega)$. The peak position is the same as that in the spectra shown in Figs. 13–16. Since the density-density correlation function Π_{33} can be measured more easily than the phase correlation function Π_{22}, and may be the most useful way of observing the Goldstone mode.

VII. SUMMARY AND DISCUSSION

In this paper we have investigated the BCS-BEC crossover in the superfluid phase of a uniform gas of Fermi atoms

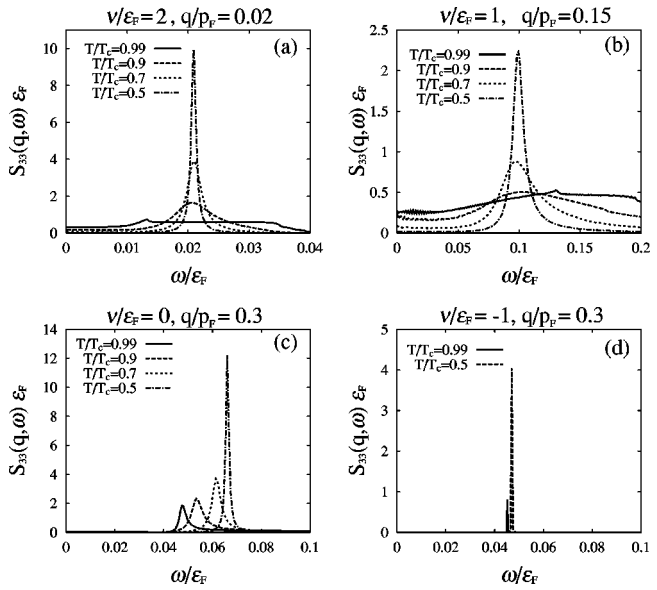

FIG. 19. Spectrum of the dynamic structure function $S_{33}(\mathbf{q},\omega)$ in the BCS-BEC crossover. The momentum values are the same as in Figs. 13–16. The sharp peak structure is the Goldstone phonon mode.

with a Feshbach resonance. Going past the simple weak-coupling mean-field theory, we included the strong-coupling effect originating from the pairing interaction associated with a Feshbach resonance. We have extended our previous work [12–14] at and above T_c to the superfluid region below T_c. We showed that the superfluid order parameter continuously changes from the Cooper-pair amplitude $\Delta = U\Sigma_{\boldsymbol{p}}\langle c_{-\boldsymbol{p}\downarrow}c_{\boldsymbol{p}\uparrow}\rangle$ in the BCS regime to the square root of the number of condensed b molecules $\phi_m = \langle b_{\boldsymbol{q}=0}\rangle$ associated with the Feshbach resonance in the BEC regime, as one lowers the threshold energy 2ν of the Feshbach resonance. In the intermediate regime in the BCS-BEC crossover, superfluidity is described by the composite order parameter $\tilde{\Delta} \equiv \Delta - g_r\phi_m$ [8,9,12].

The Goldstone mode is one of the most fundamental phenomena in an ordered system with spontaneous breakdown of a continuous symmetry. In this paper, we investigated how the Anderson-Bogoliubov mode, which is the Goldstone mode in the BCS superfluidity, changes to the Bogoliubov phonon mode in the BCS-BEC crossover. The velocity of the Goldstone mode v_ϕ strongly depends on the threshold energy 2ν, and decreases as one approaches the BEC regime. The Anderson-Bogoliubov phonon mode may be a useful way of monitoring the BCS-BEC crossover. Since it is difficult to strongly modify the strength of the pairing interaction in metallic superconductors, the tunable pairing interaction associated with the Feshbach resonance in Fermi atomic gases gives one a unique tool to clarify the physics in the BCS-BEC crossover region.

We also investigated the damping of the Goldstone mode. The fermion Landau damping of the Goldstone mode due to coupling to fermions becomes weak far below T_c, reflecting the fact that the thermal excitation of fermion quasiparticles is negligible. This damping effect is always weak in the BEC regime because the system is then dominated by b molecules, with the suppression of the Fermi quasiparticle spectrum. Thus, except in a small region near T_c in the BCS regime, the Goldstone mode appears as a strong resonance both in the spectrum of the phase correlation function and in the excitation spectrum of b bosons. As a way to experimentally observe this Goldstone mode, we noted that since the amplitude and phase fluctuations couple with the density-fluctuations, one can observe this collective mode in the spectrum of the density-density correlation function $\Pi_{33}(\mathbf{q},\omega_+)$. In cigar-shaped trapped Fermi gases, the direct observation of a density fluctuation pulse might be possible, in analogy with the observation of a Bogoliubov phonon in a superfluid Bose gas with a very weak axial trapping potential [50]. We also note that two photon Bragg scattering experiments provide a convenient way of studying density fluctuations in a trapped atomic gas [49–52]. In such experiments, $\mathrm{Im}\Pi_{33}(\mathbf{q},\omega)$ is measured directly, rather than $S_{33}(\mathbf{q},\omega)$ [52].

It is important to remember that our treatment of the BCS-BEC crossover leaves out several important contributions. In our calculation of various response functions, we always ignored the fermion self-energy arising from the coupling to the non-Bose-condensed bosons [34]. In the crossover region, these two-particle states are strongly damped. The numerical results given in Secs. V and VI show how Landau damping due to fermions decreases as we approach the BEC regime (small or negative values of ν/ε_F). This is simply because more and more fermions are forming the bound states. However, we expect new forms of damping to arise in the BEC region, namely, the Landau and Baliaev damping associated with the interaction between Bogoliubov excitations [53].

We also note that to illustrate our theory of the superfluid state, we have used a relatively weak-coupling strength parameter g_r describing the Feshbach resonance. In Sec. IV of Ref. [14], we presented calculations of the BCS-BEC crossover transition temperature for a very broad Feshbach resonance considered in Refs. [11,15]. In the case of large g_r, the crossover can occur even if the threshold 2ν is very large. In this case, the Cooper pairs dominate over the b bosons in the BEC phase.

In this paper, we have not considered the effect of a trap. The atomic density profile in the BCS-BEC crossover in a trap was recently investigated within the LDA by the authors at and above T_c [13,14], using the coupled fermion-boson model, and at $T=0$ by Perali *et al.* [28], using the strong-coupling BCS model [26]. A trap potential also leads to various discrete low-energy collective modes associated with the confined geometry, and it will be interesting to study how these collective oscillations behave in the BCS-BEC crossover. This will be the subject of a future paper, but we conclude with a few brief remarks on this. In the BCS limit of our model, one has the extensive theoretical work [31,32,53] on the Cooper-pair condensate modes in trapped Fermi gases. To be specific, we consider the quadrupole mode $\omega_Q = \sqrt{2}\omega_0$ (where ω_0 is the trap frequency of a spherical trap). This is an analog of the Goldstone phonon mode in a uniform system. If ω_Q is greater than the effective threshold $2\Delta_{\mathrm{eff}}$ for breaking up Cooper-pairs, this mode is damped and

has small spectral weight [32]. However, as one approaches the BCS-BEC crossover, the spectral weight of the fermion quasiparticles decreases, shifting to the quadrupole mode ω_Q. In the BEC limit, the mode $\omega_Q = \sqrt{2}\omega_0$ is the well-known quadrupole oscillation of a trapped Bose gas [53,54]. In this paper, we have seen that the Goldstone phonon mode in a uniform gas also persists in the BCS-BEC crossover, but the phonon velocity changes. In contrast, the quadrupole mode frequency does not depend explicitly on the interaction strength, having the same frequency $\omega_Q = \sqrt{2}\omega_0$ in both the BCS and BEC limits. What does change is its spectral weight and damping, which could be used as an experimental signature.

ACKNOWLEDGMENTS

Y.O. would like to thank Professor S. Takada and Professor M. Ueda for useful discussions, and the Japanese Government for financial support while a visiting professor at the University of Toronto. A.G. acknowledges financial support from the NSERC of Canada.

[1] B. DeMarco and D.S. Jin, Science (Washington, DC, U.S.) **285**, 1703 (1999).
[2] A.G. Truscott, K.E. Strecker, W.I. McAlexander, G.B. Partridge, and R.G. Hulet, Science (Washington, DC, U.S.) **291**, 2570 (2001).
[3] F. Schreck, L. Khaykovich, K.L. Corwin, G. Ferrari, T. Bourdel, J. Cubizolles, and C. Salomon, Phys. Rev. Lett. **87**, 080403 (2001).
[4] S.R. Granade, M.E. Gehm, K.M. O'Hara, and J.E. Thomas, Phys. Rev. Lett. **88**, 120405 (2002).
[5] G. Ferrari, M. Inguscio, W. Jastrzebski, G. Modugno, G. Roati, and A. Simoni, Phys. Rev. Lett. **89**, 053202 (2002).
[6] K.M. O'Hara, S.L. Hemmer, M.E. Gehm, S.R. Granade, and J.E. Thomas, Science (Washington, DC, U.S.) **298**, 2179 (2002).
[7] E. Timmermans, P. Tommasini, M. Hussein, and A.K. Kerman, Phys. Rep. **315**, 199 (1999).
[8] E. Timmermans, K. Furuya, P.W. Milonni, and A.K. Kerman, Phys. Lett. A **285**, 228 (2001).
[9] M. Holland, S.J.J.M.F. Kokkelmans, M.L. Chiofalo, and R. Walser, Phys. Rev. Lett. **87**, 120406 (2001).
[10] M.L. Chiofalo, S.J.J.M.F. Kokkelmans, J.N. Milstein, and M.J. Holland, Phys. Rev. Lett. **88**, 090402 (2002).
[11] S.J.J.M.F. Kokkelmans, J.N. Milstein, M.L. Chiofalo, R. Walser, and M.J. Holland, Phys. Rev. A **65**, 053617 (2002).
[12] Y. Ohashi and A. Griffin, Phys. Rev. Lett. **89**, 130402 (2002).
[13] Y. Ohashi and A. Griffin, Physica B **392-333**, 40 (2003).
[14] Y. Ohashi and A. Griffin, Phys. Rev. A **67**, 033603 (2003).
[15] J.N. Milstein, S.J.J.M.F. Kokkelmans, and M. Holland, Phys. Rev. A **66**, 043604 (2002).
[16] T. Loftus, C.A. Regal, C. Ticknor, J.L. Bohn, and D.S. Jin, Phys. Rev. Lett. **88**, 173201 (2002).
[17] C.A. Regal, C. Ticknor, J.L. Bohn, and D.S. Jin, Phys. Rev. Lett. **90**, 053201 (2003).
[18] P. Nozières and S. Schmitt-Rink, J. Low Temp. Phys. **59**, 195 (1985).
[19] A. Tokumitsu, K. Miyake, and K. Yamada, Phys. Rev. B **47**, 11988 (1993).
[20] C.A.R. Sá de Melo, M. Randeria, and J.R. Engelbrecht, Phys. Rev. Lett. **71**, 3202 (1993).
[21] M. Randeria, in *Bose-Einstein Condensation*, edited by A. Griffin, D. W. Snoke, and S. Stringari (Cambridge University Press, New York 1995), p. 355.
[22] R. Friedberg and T.D. Lee, Phys. Rev. B **40**, 6745 (1989).
[23] J. Ranninger, in *Bose-Einstein Condensation*, Ref. [21], p. 393.
[24] T. Kostyrko and J. Ranninger, Phys. Rev. B **54**, 13 105 (1996).
[25] F. Weig and W. Zwerger, Europhys. Lett. **49**, 282 (2000).
[26] G.M. Bruun and C.W. Clark, Phys. Rev. Lett. **83**, 5415 (1999).
[27] G.M. Bruun, Phys. Rev. A **66**, 041602 (2002).
[28] A. Perali, P. Pieri, and G.C. Strinati, e-print cond-mat/0212067.
[29] P.W. Anderson, Phys. Rev. **112**, 1900 (1958).
[30] See, for example, A. Griffin, *Excitations in a Bose-Condensed Liquid* (Cambridge University Press, New York 1993).
[31] M.A. Baranov and D.S. Petrov, Phys. Rev. A **62**, 041601 (2000).
[32] G.M. Bruun and B.R. Mottelson, Phys. Rev. Lett. **87**, 270403 (2001).
[33] G.M. Bruun and H. Heidelberg, Phys. Rev. A **65**, 053407 (2002).
[34] R. Haussmann, *Self-consistent Quantum-Field Theory and Bosonization for Strongly Correlated Electron Systems* (Springer-Verlag, New York, 1999), Chap. 3.
[35] Y. Ohashi and S. Takada, J. Phys. Soc. Jpn. **66**, 2437 (1997).
[36] Y. Ohashi and S. Takada, Phys. Rev. B **62**, 5971 (2000).
[37] See, for example, J. R. Schrieffer, *Theory of Superconductivity* (Addison-Wesley, Palo Alto, CA, 1964), Chap. 7.
[38] R. Côté and A. Griffin, Phys. Rev. B **37**, 4539 (1988).
[39] The b-boson kinetic term ($\Sigma_{\mathbf{q}} \xi_{B\mathbf{q}} b_{\mathbf{q}}^{\dagger} b_{\mathbf{q}}$) in Eq. (3.7) is, strictly speaking, a fluctuation term around ϕ_{m}. However, since the quadratic contribution to Ω is easily evaluated, it is included in Ω_{MF}.
[40] K.Y.M. Wong and S. Takada, Phys. Rev. B **37**, 5644 (1988).
[41] For details, see Sec. IV, Y. Ohashi and A. Griffin, e-print cond-mat/0302196.
[42] N. Hugenholtz and D. Pines, Phys. Rev. **116**, 489 (1959).
[43] P.C. Hohenberg and P.C. Martin, Ann. Phys. (N.Y.) **34**, 291 (1965).
[44] G. Rickayzen, *Green's Functions and Condensed Matter* (Academic Press, London, 1991), Chap. 9.
[45] J.R. Engelbrecht, M. Randeria, and C.A.R. Sa de Melo, Phys. Rev. B **55**, 15 153 (1997).
[46] See, for example, G. Schön, *Nonequilibrium Superconductivity*, edited by D.N. Langenberg and A.I. Larkin (Elsevier Science, Amsterdam, 1986), Chap. 13.
[47] A. Schmid, Prog. Photovoltaics **8**, 129 (1968).
[48] T. Jujo, Y. Yanase, and K. Yamada, J. Phys. Soc. Jpn. **69**, 2240 (2000).

[49] W. Ketterle, in *Coherent Atomic Matter Waves*, Proceedings of Les Houches 1999 Summer School, Session LXXII, edited by R. Kaiser, C. Westbrook, and F. David (Springer-Verlag, New York, 1999).

[50] M.R. Andrews, D.M. Kurn, H.-J. Miesner, D.S. Durfee, C.G. Townsend, S. Inouye, and W. Ketterle, Phys. Rev. Lett. **79**, 553 (1997); **80**, 2967 (1998).

[51] F. Zambelli, L. Pitaevskii, D.M. Stamper-Kurn, and S. Stringari, Phys. Rev. A **61**, 063608 (2000).

[52] J. Steinhauer, R. Ozeri, N. Katz, and N. Davidson, Phys. Rev. Lett. **88**, 120407 (2002).

[53] C.J. Pethick and H. Smith, *Bose-Einstein Condensation in Dilute Gases* (Cambridge University Press, New York, 2002), Chap. 14.

[54] S. Stringari, Phys. Rev. Lett. **77**, 2360 (1996).